Fuel 271 (2020) 117600

Contents lists available at ScienceDirect

Fuel

journal homepage: www.elsevier.com/locate/fuel

Review article

Characteristics of flash boiling and its effects on spray behavior in gasoline direct injection injectors: A review

Mengzhao Chang[a,1], Ziyoung Lee[b,1], Sungwook Park[c], Suhan Park[d,*]

[a] Department of Mechanical Engineering, Graduate School of Chonnam National University, 77 Yongbong-ro, Buk-gu, Gwangju 61186, Republic of Korea
[b] Department of Mechanical Convergence Engineering, Graduate School of Hanyang University, 222 Wangsimni-ro, Seongdong-gu, Seoul 04763, Republic of Korea
[c] School of Mechanical Engineering, Hanyang University, 222 Wangsimni-ro, Seongdong-gu, Seoul 04763, Republic of Korea
[d] School of Mechanical Engineering, Chonnam National University, 77 Yongbong-ro, Buk-gu, Gwangju 61186, Republic of Korea

ARTICLE INFO

Keywords:
Flash boiling
GDI injector
Spray characteristics
Atomization
Evaporation
Two-phase fluid model

ABSTRACT

The flash boiling phenomenon occurs when the ambient pressure around fuel is lower than the saturation pressure. This is followed by the formation and growth of bubbles. Flash boiling has been regarded as a promising method to improve the atomization of fuel sprays and to reduce emissions without a high-pressure injection system, which has recently become a popular topic. Therefore, it is necessary to summarize the current research status of flash boiling sprays. This review seeks to provide on overall understanding of flash boiling sprays in gasoline direct injection (GDI) injectors and includes theoretical, experimental, and numerical studies relevant to the flash boiling process. The effects of the degree of superheating and injector configuration, which includes the spacing angle, nozzle number and nozzle length, on spray behavior under flash boiling conditions are analyzed. Furthermore, in order to gain a deep understanding of the collapse mechanism of the spray, the formation of the collapse is explained from several aspects, including the velocity field, temperature field, vapor concentration field, and droplet diameter. A thorough understanding of flash boiling spray behaviors and the collapse mechanisms can help further technological applications, such as injector design and injection strategies. Finally, an overview of the available theoretical models and their applications is presented, which provides a simple and concise method of understanding flash boiling spray behavior.

1. Introduction

Recently, gasoline direct injection (GDI) injectors with a maximum injection pressure of 70 MPa have been developed [1]. To meet increasingly stringent requirements, GDI injectors improve combustion efficiency and reduce emissions by quickly reaching high pressures. The increase in injection pressure is believed to be a key means of improving the atomization process, which affects the mixture formation, combustion and soot emission in GDI engines [2,3]. Previous scientific research has found that the particle number and mass can be reduced by improved spray atomization, faster evaporation, and better mixture formation for high-pressure injection [4]. Moreover, the flash boiling phenomenon is considered to be a possible method of producing an optimal fuel spray with finer droplets and uniform fuel/air mixture. Flash boiling features a two-phase flow that constantly generates vapor bubbles inside the liquid spray. This occurs when liquid fuel is injected into an ambient environment below its saturation pressure. The importance and mechanism of the flash boiling phenomenon on fuel spray was stablished by Brown and York [5]. The primary purpose of the study was to analyze the pressure dispensing of aerosols in which liquid jets were dominantly atomized by flash boiling. Rapid bubble growth in low-pressure regime resulted in bubble explosions at some distance from the nozzle. However, while such behavior was suitable in the low degree of superheating regime, it was difficult to assess the flash sprays in engine applications. Thus, flash boiling caused by a high degree of superheating for engine operating conditions has been widely studied since the 1980s [6–8]. Owing to the significant potential of flash boiling to improve combustion efficiency and reduce emissions, flash boiling spray in engines has once again become a prevalent topic of research.

Fig. 1 shows the thermodynamic processes of different types of

Abbreviations: GDI, gasoline direct injection; ASOI, after start of injection; SD, superheating degree; LIEF, laser induced exciplex fluorescence; PDA, phase Doppler; LD, laser diffraction; SMD, sauter mean diameter; L/D, ratio of nozzle length and nozzle diameter; RNG, re-normalisation group model; TAB, Taylor analogy breakup model; HRM, homogeneous relaxation model

* Corresponding author.
E-mail address: suhanpark@jnu.ac.kr (S. Park).
[1] These authors contributed equally to this paper.

https://doi.org/10.1016/j.fuel.2020.117600
Received 17 December 2019; Received in revised form 6 March 2020; Accepted 8 March 2020
Available online 17 March 2020

Nomenclature

t_{asoi}	time after start of injection ms
P_a	ambient pressure MPa
P_s	saturation pressure MPa
T_{fuel}	fuel temperature K
T_s	saturation temperature K
P_a/P_s	ambient-to-saturation pressure
R_P	saturation-to-ambient pressure

injections in a pressure temperature diagram [9]. According to the thermodynamic pathway of the liquid during injection, injections can be divided into three types; liquid injection, superheat injection and supercritical injection. Liquid injection occurs when the ambient pressure is well above the liquid saturation pressure. In this region, inertia, viscosity, surface tension, and aerodynamic forces affect the spray characteristics. Superheat injection occurs when high-temperature liquid fuel is injected into a low-pressure environment. When the subcooled fuel flows at high speed before arriving at the exit of the nozzle, the pressure around the fuel decreases rapidly. As the pressure becomes lower than the saturation pressure, the flash boiling phenomenon occurs [10–12]. The atomization in this region is mainly influenced by the growth and explosion of bubbles [13]. Further increasing the fuel pressure and temperature beyond the critical point results in flash boiling in the supercritical region; however, supercritical injection is rarely encountered in the operating conditions of internal combustion engines [14].

In the actual operating conditions of the internal combustion engine, the internal pressure of the cylinder can decrease to 0.02 MPa in the early injection strategy, and the fuel temperature can increase to over 150 ℃ under high load ignition conditions [15]. Many studies have shown that flash boiling occurs under typical in-cylinder ambient conditions [16–19]. Flash boiling causes rapid phase transition of liquid fuel to vapor fuel, which leads to volume expansion and changes in the spray width and penetration [20]. Therefore, through the reasonable design and optimization of the injector, chamber, and injection timing, the advantages of flash boiling may be better utilized and the disadvantages avoided. In addition, it was found that a more uniformly distributed mass and smaller drop sizes could be produced under flash boiling conditions without high injection pressure [21–23]. As a result, flash boiling for GDI engines is becoming a prevalent topic of research.

Guo et al. [18] investigated the effect of flash boiling on the microscopic and macroscopic spray characteristics in a single cylinder optical GDI engine. They found that flash boiling occurred at room temperature (RT) under idle operation, and the Sauter mean diameter (SMD) reduced by 33.2% as the fuel temperature increased from 20 ℃ to 60 ℃. In addition, they used the Rosin-Rammler function as follows to describe the droplet size distribution:

$$1 - Q = \mathrm{EXP} - (D/X)^q \quad (1)$$

where Q is the fraction of the volume contained in a drop with a diameter less than D, X is the mean diameter, and q represents the droplet uniformity. Using this equation, they found that increasing the fuel temperature improved droplet uniformity. Yang et al. [24] investigated the combustion characteristics of flash boiling spray under cold start conditions; they found that flash boiling sprays improved the partial burn and misfire, and the stable stage of the engine decreased from 30 cycles to 2 cycles. In addition, owing to the lower yellow flame luminosity and higher blue flame propagation rate at flash boiling conditions, the particulate number (PN) emission was reduced, and higher the indicated mean effective pressure (IMEP) was increased. Huang et al. [25] examined the effect of heated ethanol fuel on the combustion and emission performance of spark-ignition (SI) engines at medium load. A significant reduction in the indicated specific carbon monoxide (ISCO) and hydrocarbon (ISHC) was achieved by heating the fuel, and was attributed to the complete combustion caused by improved evaporation, local–cooling, and fuel impingement [26]. However, the indicated specific nitric oxides ($ISNO_x$) emission increased slightly, which might have been caused by the increased combustion temperature resulting from the heated fuel.

Vaporization that occurs under depressurization conditions is often referred to as flash boiling or cavitation. The temperature (or pressure) level is considered to be the fundamental difference between 'flash boiling' and 'cavitation'. Flash boiling is more like a boiling process for hot fuel and is usually accompanied by high thermal non-equilibrium. In particular, the bubble growth rate is limited by the heat transfer rate of the interphase. Cavitation occurs at a relatively low temperature (or pressure), in which the density of the vapor is low, and the lower superheating degree is sufficient to maintain the evaporation process. In this case, bubble expansion is mainly controlled by mechanical non-equilibria [27]. In reality, mechanical and thermal non-equilibrium exist simultaneously in a depressurization process, but few investigations have considered the effects of cavitation while studying flash boiling.

As mentioned previously, flash boiling is regarded as a potential method to improve the atomization effect of the fuel spray, improve the power output and reduce particulate emissions, all of which provide a new direction for the design of injection strategies and injectors [24,25,28,29]. This review is intended to provide an overall understanding of the flash boiling phenomenon in GDI engines. The specific content includes the basic theory of flash boiling, experimental apparatuses, experimental characteristics and mechanism of flash boiling spray, and current state of the construction of the flash boiling model.

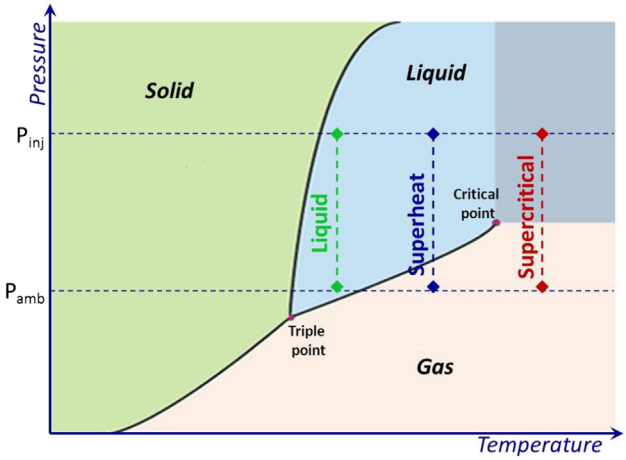

Fig. 1. Thermodynamic processes during different types of injections [9].

2. Theory of flash boiling

2.1. Nucleation

Atomization in superheated fluids mainly occurs through nucleate boiling; Bubble nucleation is the rate-controlling process for both the transition to full flash boiling and for the lateral spread of the spray. Therefore, understanding the mechanism of bubble formation is especially important in the experimental study and model establishment of flash boiling [30]. The bubble nucleation process can be divided into homogeneous nucleation and heterogeneous nucleation. Fig. 2 shows the schematics of the two nucleation processes [27]. During homogeneous nucleation, if the liquid is heated to a metastable state, bubbles are generated everywhere inside the liquid. During heterogeneous nucleation, bubbles in a superheated liquid in a metastable state develop adjacent to the solid surface of the container [27,31,32]. However, homogeneous nucleation in particular is not easily achieved, except

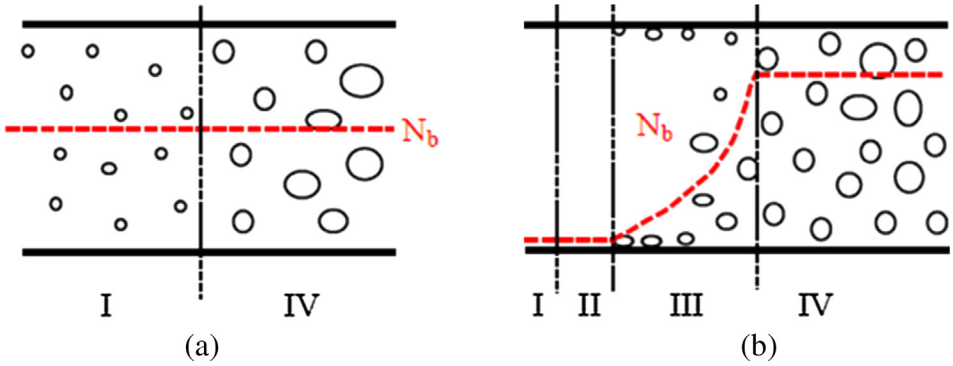

Fig. 2. Schematic of homogeneous nucleation (a) and heterogeneous nucleation (b).

under carefully controlled laboratory conditions. In most actual situations, the metastable liquid will undergo a phase change before it reaches the homogeneous nucleation limit. This is called flashing inception mechanism heterogeneous nucleation. In classical nucleation theory, the rate of nucleation (i.e., the number of stable vapor nuclei generated per unit volume and time) is expressed as [30]

$$J_{CNT} \propto \sqrt{\frac{2\sigma}{\pi m}} \exp\left(-\frac{4}{27}\frac{\theta^3}{(lnR_P)^2}\right) \quad (2)$$

where θ is the surface tension, and R_p is the ratio between the saturation pressure at the fuel injection temperature and ambient pressure. Experimental investigations have proved that suppression of the nucleation rate inside the nozzle accounts for the non-collapse features [33,34].

2.2. Evaporation wave and shock wave

Fig. 3 shows a schematic of an evaporation wave and a shock wave. Evaporation waves may occur under certain conditions in which a metastable or superheated liquid undergoes a sudden phase transition in a narrow and observable region [35]. When the jet occurs under flash boiling conditions, a sudden phase transition occurs at the surface of the central liquid core and an oblique evaporation wave forms, causing the velocity of the superheated liquid to tilt the evaporation front (1 → 2). In extreme conditions, such as extremely high injection pressures or very low ambient pressure, the normal velocity component of the two-phase flow is sonic compared to the evaporation wave front frame. Then, the two-phase flow expands freely from the oblique evaporation wave to attain supersonic velocities and comprises the expansion process (2 → 3). Finally, a regular compression shock wave forms and is accompanied by the end of the supersonic expansion process (3 → 4) [36]. However, in the actual process of GDI engine operation, extreme conditions are very unlikely to occur (ambient pressure is usually no more than 10 kPa). Consequently, there has not been much research on the shock wave phenomenon of GDI injector spray to date.

2.3. Collapse

Spray collapse is referred to as the spatial contraction of a nominal spray. Spray collapse can be affected or induced by flash boiling, but can also be enforced in non-superheated conditions by a simple increase in the flow hole number of multi-hole injectors [37]. Generally, it is believed that a reduction in the internal pressure of the spray is the main cause of the collapse [38–40]. Moon et al. [41] found that the pressure inside the spray decreases as the fuel temperature increases by using pressure sensor that was installed 3 mm directly below the nozzle as shown in Fig. 4. Wu et al. [42,43] have conducted a lot of research on the collapse mechanism of multi-hole GDI injectors, and proposed a model of the collapse mechanism. Fig. 5(a) shows that they found the plumes began to expand as the fuel temperature increased, followed by the formation of a closed area at the center of the plumes. Finally, the plumes all moved to the spray center. Fig. 5(b) shows that their belief that when a closed area at the center of the plumes was formed due to plume expansion, the gas could not move from the outside to the closed central region. As the spray developed farther downward, a pressure difference between spray exterior and the spray center was produced. Under the action of external air pressure, the spray plume moved to the spray center and collapse occurred. However, we consider that real experimental data is needed to explain the collapse mechanism more accurately. Li et al. [17] and Guo et al. [28] also studied the collapse mechanism of multi-hole flash boiling sprays. They found that the local static pressure significantly increased at the balance position by simulating the motion process after the fuel was injected from the nozzle. The increased static pressure was beyond the local saturation pressure, fulfilling the condition for vapor condensation. They postulated that the vapor condensation near the nozzle exit was the primary cause for the collapse under flash boiling conditions. In addition to research on the flash boiling spray of single-hole and multi-hole GDI injectors, there are also some studies on hollow cone piezoelectric GDI injectors, which can provide a deeper understanding of the mechanism of spray collapse. Under low superheat conditions, the spray presents a hollow conical umbrella shape. However, under high superheat conditions, the hollow cone becomes smaller and a rapidly developing plume is formed along the spray axis owing to the oblique evaporation wave induced by the inward expansion and merging of the spray [44,45].

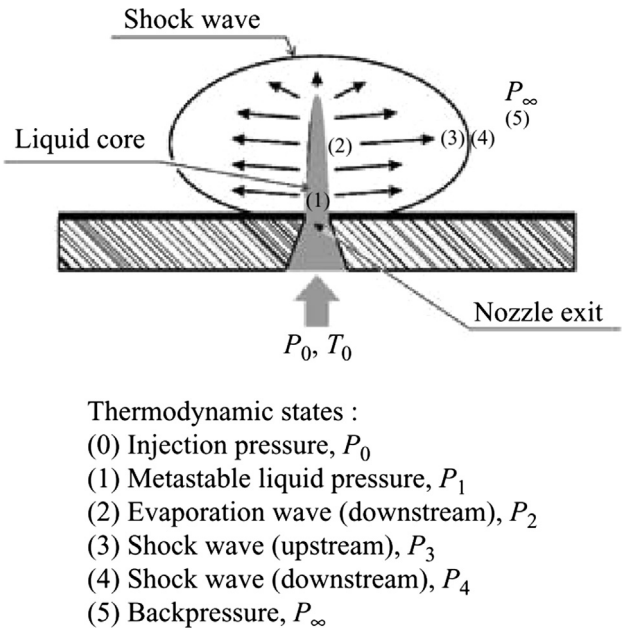

Fig. 3. Schematic of an oblique evaporation wave and shock wave [36].

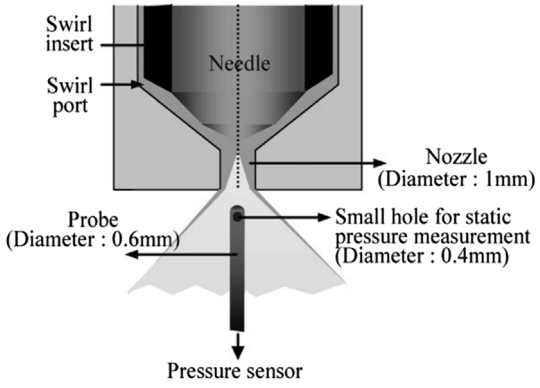

Fig. 4. Experimental setup for the measurement of interior static pressure inside [41].

2.4. Superheating degree and ambient-to-saturation pressure

The ambient-to-saturation pressure (P_a/P_s) is defined as the ratio of the ambient pressure to the saturation pressure of the fuel. The superheating degree (SD or T_f-T_b) is the difference between the fuel temperature and temperature at the fuel boiling point. The ambient-to-saturation pressure and superheating degree are commonly used as characteristic parameters to describe the structural transformation of flash boiling spray. It has been found that the superheating degree is linear with the logarithm of the ambient-to-saturation pressure, which indicats that these two characteristic parameters are similar in principle [46]. Apart from P_a/P_s and SD, R_P is also used by researchers to express the degree of superheating, which is defined as the ratio of the saturation pressure to the ambient pressure of the fuel.

3. Experimental apparatus and methods

Two important conditions required for flash boiling to occur are low ambient pressure and high temperatures. Typically, a closed chamber and vacuum pump are used to create a low-pressure environment. The temperature of the fuel inside the injector is usually raised indirectly by heating the chamber head. Among the many heating methods, provision of circulating hot fluid to the interior of the chamber head is generally considered the preferred method for achieving the uniform and stable heating of fuel [42,46]. To visualize the flash boiling spray and study the motion and atomization characteristics, the most commonly used experimental methods are Schlieren, Mie scattering, laser-induced exciplex fluorescence (LIEF), and phase Doppler anemometry (PDA). These methods are summarized in Tables 1 and 2.

3.1. Schlieren visualization method

The Schlieren technique is the most common method used to observe vapor phase sprays. This method employs refracted light rays, which translate changes in density into changes in the intensity of light. Finally, regions of light and dark, as recorded by a camera, are produced. The Schlieren light path is mainly composed of a point light source, two concave mirrors, a knife-edge and a high-speed camera. Fig. 6 shows a typical schematic of the Z-type Schlieren setup.

As it can be difficult to assemble and align the Schlieren setup, the setup of the Schlieren system is presented here. The primary components of the Schlieren setup in this experiment are two spherical focusing mirrors. In order to guarantee the accuracy of the Schlieren system, the two concave mirrors need to have longer focal lengths. The "f-number" of a mirror is the ratio of the focal length to the diameter of the mirror. A recommended entrance/exit angle for the beams is between 15° and 20°, as shown in Fig. 6.

Place the two mirrors on the optical platform, facing each other at a distance of approximately double the focal length. The mirrors will need to be elevated from the table surface in order to align their centerlines with the height of the light source. The projection point of the center of the two concave mirrors on the optical platform is taken as the origin. Two tapes are attached to the optical platform from the two origins such that the two tapes and the connection between the two origins form a zigzag shape. The two angles of the zigzag shape are ensured to be in the range of 15°–20°. Then, the light source is assembled by placing it along the tape at the focus of the first mirror and point the light source towards the first mirror. Next, a clean sheet of

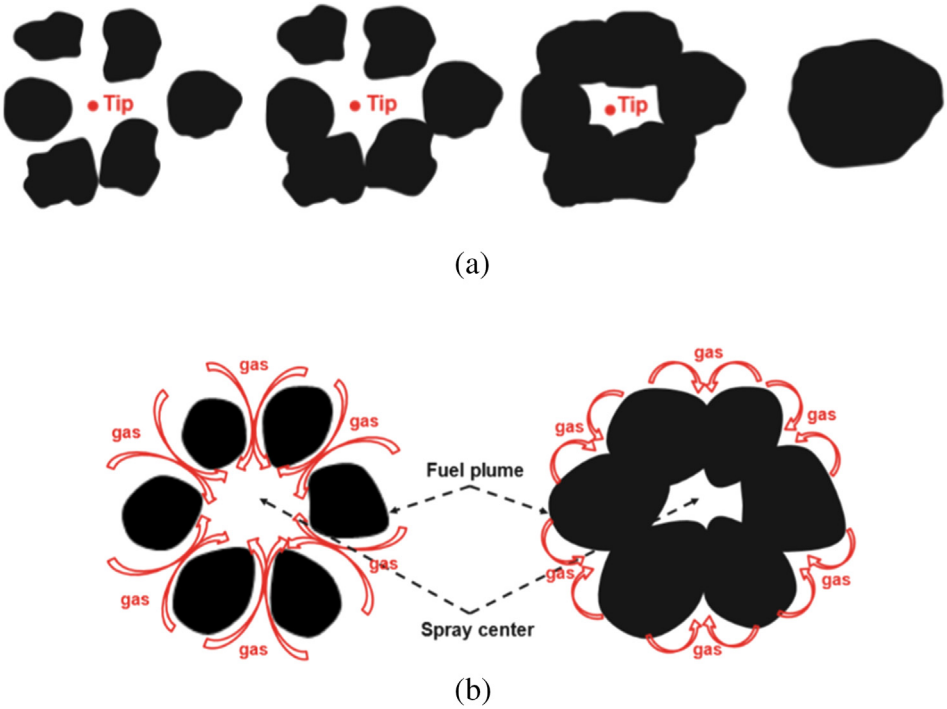

Fig. 5. Process of spray collapse and the collapse mechanism [42,43].

Table 1
Summary of previous studies on flash boiling sprays under different degrees of superheating.

Year	Authors	Working fluid	Methods	Main contribution
2007	Moon et al. [41]	Gasoline, i-octane	–	The effect of fuel temperature on air pressure inside the spray was studied
2019	Wu et al. [42]	*n*-Hexane	Mie scattering, Radial laser	The mechanism of collapse was analyzed by establishing an air motion model
2017	Guo et al. [18]	Gasoline	Mie scattering, PDPA	The effects of flash boiling on microscopic spray characteristics (mean diameter, droplet size distribution) were investigated
2012	Zeng et al. [16]	Gasoline, Methanol, Ethanol	Mie scattering,	Dimensionless analysis was applied to investigate the macroscopic spray characteristics of an SDI engine under a board of SIDI engine conditions.
2018	Li et al. [17]	Gasoline	Mie scattering, PDPA	The collapse of multi-jet flash-boiling sprays was induced by vapor condensation at the nozzle exit
2012	Zeng et al. [46]	*n*-Hexane, Methanol, Ethanol	Mie scattering, LIEF	A standard for distinguishing three regions (subcooled region, transitional region, flare flash boiling region) was determined by using Pa/Ps. The effect of Pa/Ps on spray and evaporation characteristics of spray were studied
2017	Montanaro et al. [79]	Iso-octane	Mie scattering, Schlieren	Liquid phase spray and vapor phase spray were compared under flash boiling conditions
2013	Aleiferis et al. [15]	*iso*-octane, *n*-pentane, gasoline, ethanol, *n*-butanol	Mie scattering, Shadowgraph, PDA	Spray development of *iso*-octane, n-pentane, gasoline, ethanol and n-butanol were compared from a multi-hole injector under hot fuel conditions
2014	Wood et al. [50]	*n*-Heptane	Mie scattering, PDA	An ever-increasing database of knowledge on the behavior of multi-hole GDI sprays under flash boiling conditions was built
2012	Zhang et al. [80]	*n*-Hexane	PIV	The spray velocity fields in cross-sectional direction under various superheated conditions were investigated
2013	Zhang et al. [81]	*n*-Hexane	PIV	The spray velocity fields in the axial direction under various superheated conditions were investigated.
2014	Zhang et al. [51]	*n*-Hexane 90.5% + FB 0.5% + DEMA 9%	LIEF	The evaporation of flash boiling sprays was investigated by measuring the 2D distributions of liquid and vapor mass, vapor concentration, and liquid temperature
2018	Guo et al. [34]	*n*-Hexane	Shadowgraph	External flashing was observed and it was considered as a potential method to mitigate collapse; effect of nucleation rate on radial expansion was studied
2019	Li et al. [33]	Proane, *n*-hexane, *iso*-octane	Shadowgraph	Flashing propane sprays presented non-collapse features under elevated-ambient-pressures owing to the prohibition of nucleation and bubble growth
2016	Wei et al. [82]	Gasoline, M20, M40	Schlieren	The spray characteristics of MF– gasoline blends M20, M40 and gasoline were investigated under various ambient pressures and fuel temperatures
2014	Huang et al. [39]	Ethanol	Shadowgraph	Droplet explosion occurred when the degree of superheating exceeded 14 °C. Evaporation characteristics were compared using pixel intensities.
2016	Huang et al. [83]	Ethanol, Gasoline	Shadowgraph	Not only the spray evaporation modes but also the breakup mechanisms changed with the fuel temperature
2018	Lacey et al. [38]	Iso-octane, propane	Schlieren	New criteria for both spray collapse and plume interaction were proposed
2018	Li et al. [29]	p-Xylene	UV-LAS	The effects of surface evaporation and flashing evaporation on evaporation of flash boiling spray were identified
2017	Wu et al. [84]	N-Pentane	Shadowgraph	Larger internal bubble volume fraction resulted in faster disintegration process of the near nozzle fuel jet
2018	Yang et al. [58]	N-Hexane	Shadowgraph	The mass flow rate of flash boiling spray is not significant because of the acceleration of the spray by flash boiling breakup effects
2017	Guo et al. [28]	Gasoline	Mie scattering, PDA	The characteristics of the two collapse modes were discussed at elevated ambient pressure conditions and in flash boiling conditions

Table 2
Summary of previous studies on flash boiling sprays with different injector configurations.

Year	Authors	Working fluid	Methods	Main contribution
2016	Wu et al. [43]	*n*-Hexane	Shadowgraph	Plume expanded when shifted from subcooled to flare flash boiling; Shorter nozzles led to wider sprays under all injection conditions owing to promoted jet breakup, resulting from increased axial and radial velocities
2017	Wu et al. [57]	N-pentane	Shadowgraph	A longer nozzle led to more in-nozzle bubbles due to longer time for bubble growth; a nozzle with round inlet corner inhibited bubble inception
2018	Wu et al. [85]	*n*-Hexane	Shadowgraph	Stronger restriction effect of longer nozzle wall led to weaker spray primary breakup and narrower near nozzle spray. Stronger in-nozzle fuel evaporation of longer nozzle led to faster primary breakup and wider spray
2018	Zhang et al. [86]	0# diesel	Shadowgraph	The internal flow and subsequent atomization were analyzed using a 10-times scaled-up transparent acrylic model nozzle with different geometries
2019	Guo et al. [61]	N-Hexane	Shadowgraph	Flashing sprays from single-hole and five-hole GDI injectors were studied; relationship between spray collapse and radial jet expansion was revealed
2019	Xu et al. [62]	N-pentane	Mie scattering (Laser sheet)	A secondary plume was generated by side-collision of two primary plumes in the spray central region under some flash-boiling conditions
2013	Yang et al. [59]	Gasoline	Mie scattering	The overlap region of adjacent plumes played an important role in the transformation of flash boiling sprays
2016	Kra¨mer et al. [37]	N-pentane, N-hexane, N-heptane, N-octane, N-decane	Mie scattering	Spray collapse can be affected or induced by flash boiling but also enforced at non-superheated conditions by a simple increase in the flow hole number at multi-hole injectors
2010	Serras-Pereira et al. [87]	Gasoline, *iso*-octane, *n*-pentane	Shadowgraph	Similar spray formations at near-nozzle location were seen by comparing real-size transparent nozzle with real injector; superheating degree has more effect on jet disintegration and atomization than cavitation

white paper is prepared, which is a very useful instrument for alignment. To make the alignment easier, a circle of the same size as the mirrors is drawn on the paper. At this point, it may be helpful to dim the lights in the laboratory or turn them off entirely. Carefully the distance of the light source from the mirror is adjusted until the light beam diameter reflected off the first mirror equals the diameter of the mirror. This should be tested using the paper prepared earlier. The angle of the first mirror is adjusted using the rotation and tilt controls so that the beam passes through the chamber (i.e., the test area) orthogonal to the chamber surface. The camera is then placed a little farther from the focus of the second mirror along the tape to ensure that the knife edge can be mounted at the focal position. The injector is then installed in the chamber, and the position of the camera and angle of the mirror are adjusted until the image formed on the screen is sufficiently large. The focus of the camera is carefully adjusted until the injector tip becomes distinguishable, along with the exposure, resolution and frame rate of the camera. The position and focus of the camera are continued to be adjusted again until the image is a complete circle with a clear projection of the injector tip observed by the camera. The camera is rather sensitive to light; therefore, so the brightness of the light source should be lowered to avoid saturating the camera sensor.

Once the system is properly aligned and focused, the knife-edge is slowly placed at the focus of the second mirror. When the knife-edge is perfectly aligned with the focus, the brightness of the image will be evenly dimmed. However, if the image is dimmed on the same side as the knife-edge, then the knife-edge is too close to the second mirror. If the opposite occurs, it is too far away. The position of the knife-edge should then be slowly adjusted, until the image is evenly dimmed as the knife-edge is moved into the light beam. More details about the setup for the Schlieren system can be found in Settles' book [47].

3.2. Laser-induced exciplex fluorescence method

Fig. 7 shows the experimental apparatus based on the laser-induced exciplex fluorescence (LIEF). The LIEF technique, which has the capability of distinguishing between liquid phase spray and vapor phase spray, is used to investigate the heat and mass transfer processes in which a large amount of liquid and vapor coexist and interfere with each other. The monomer (M) and exciplex-forming molecule (G) are added to an optically transparent base fuel. The phase separation can be measured based on the photochemical reaction as follows [48]:

$$M^* + \mathrm{G} \leftrightarrows E^* \tag{3}$$

where M^* and E^* are the excited monomer and exciplex, respectively. The exciplex (E^*) is mainly formed in the liquid phase owing to the short molecule-to-molecule distance. As a result, the exciplex (E^*) fluorescence represents the liquid phase of the spray, while the monomer (M) fluorescence represents the vapor phase of the spray. It is the difference in the fluorescence wavelength between the exciplex (E^*) and monomer (M) that enables measurement of the liquid and vapor phase sprays.

The vapor concentration and liquid temperature can be obtained by quantitatively analyzing the liquid and vapor fluorescence. The laser-induced fluorescence (LIF) intensity at wavelength λ_1 can be written as [49]:

$$I_{LIF} = K_{opt} K_{spec} V_C I_o C e^{\beta(\lambda_1)/T} \tag{4}$$

The quenching process, in particular, has a very minor impact on the fluorescence intensity in an oxygen-free environment and can be neglected. The vapor concentration can be calculated by simplifying Eq. (4) to:

$$I_{LIF} = K(\lambda, T)C \tag{5}$$

where C is the molecular concentration and K is the proportionality factor.

The temperature distribution of the liquid phase spray can also be

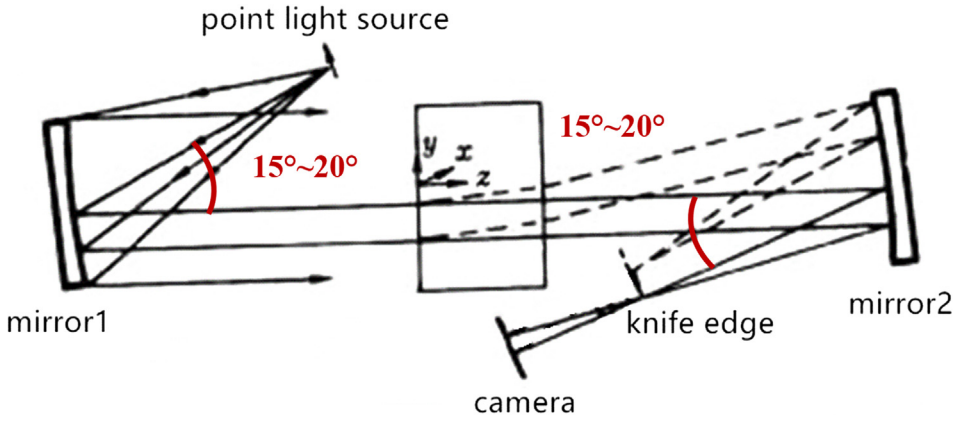

Fig. 6. Schematic of a typical Schlieren setup.

obtained by the following calculation. The fluorescence intensity ratio of two wavelengths of liquid fluorescence is given by:

$$R = \frac{K_{opt,\lambda_2} K_{spec,\lambda_2} V_c I_0 C e^{\beta(\lambda_2)/T}}{K_{opt,\lambda_3} K_{spec,\lambda_3} V_c I_0 C e^{\beta(\lambda_3)/T}} = k e^{\frac{\beta(\lambda_2)-\beta(\lambda_3)}{T}} \tag{6}$$

By choosing a reference temperature T_o, the constant K can be eliminated:

$$\ln\left(\frac{R(T)}{R(T_0)}\right) = (\beta(\lambda_2) - \beta(\lambda_3))\left(\frac{1}{T} - \frac{1}{T_0}\right) = \Delta\beta\left(\frac{1}{T} - \frac{1}{T_0}\right) \tag{7}$$

The constant $\Delta\beta$ can be calibrated and the distribution of the liquid temperature obtained by this equation.

4. Experimental study of flash boiling

4.1. Effect of superheating degree on the characteristics of flash boiling spray

Wood et al. [50] studied the behavior of multi-hole GDI sprays under flash boiling conditions. Fig. 8 shows that as the superheating degree is increased from a non-superheated state to a high level of superheat, there are significant changes in the morphology of the spray. The upper row of Fig. 8 shows the spray pattern in the vertical direction. At and SD of −12 ℃, even under non-superheated conditions, there is a widening of the spray plumes. With a low level of superheat (SD = 12 ℃) the entrainment of the fuel into recirculating vortices appears at the spray tip, where further widening of the individual spray

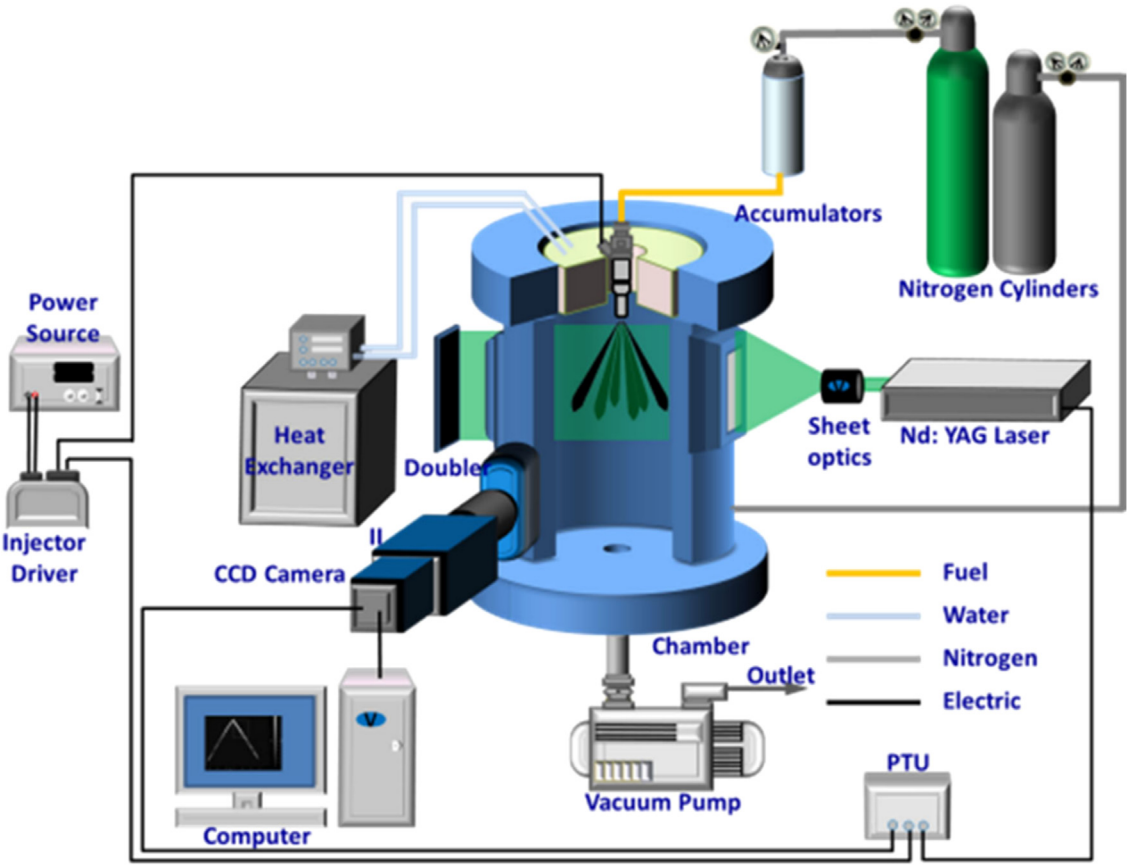

Fig. 7. Experimental apparatus based on laser-induced exciplex fluorescence [48].

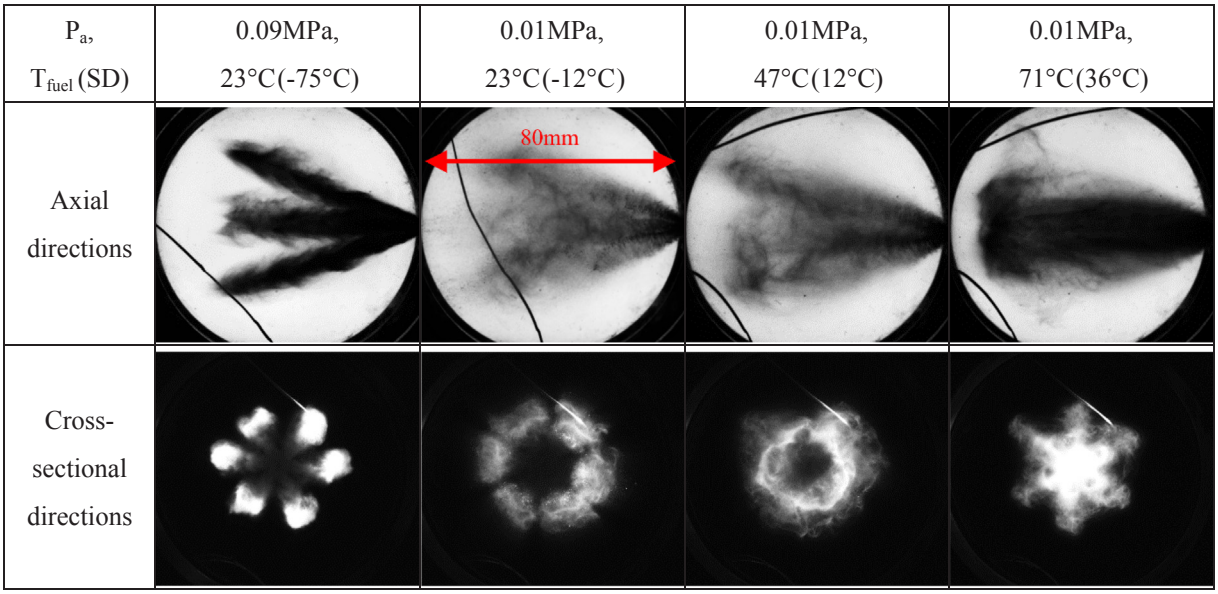

Fig. 8. Spray pattern evolution in the axial directions and cross-sectional direction (Fuel: *n*-heptane, P_{inj} = 10 MPa, t_{ASOI} = 1.1 ms, Distance of cross section to injector tip: 40 mm. As the SD increases, the plume widens, and the plumes interact and move toward the spray center) [50].

plumes and partial collapse can be seen. The vortices can be more clearly seen in the velocity field shown in Fig. 9. At and SD of 36 ℃, the original six spray plumes are completely destroyed and form a single central spray. The bottom row of Fig. 8 shows the spray pattern in the horizontal direction. The images were taken at an axial distance of 40 mm from the injector tip. At and SD of −12 ℃, a standard spray with six individual spray plumes is shown. At an intermediate superheat level (SD = 12 ℃) the spray plumes migrate to other locations and the interaction between the spray plumes is strengthened, causing them to form a closed circular pattern. At an SD of 36 ℃, the spray collapses and moves to the center of the plumes. The formation of interstitial streams in the gaps between the original spray plumes can also be seen.

Fig. 9 shows the velocity profile downstream of the nozzle tip. In a lower superheat condition (SD = 18 ℃), the spray plumes can be clearly identified in the flow fields and the maximum particle velocity in the midstream of the spray is around 50 m/s. By further increasing the SD to 28 ℃, a high velocity is observed between the plumes because of the plume interactions. Two obvious vortices are consistently present near the interface between the spray plumes and surrounding gas. The fuel spray is driven to the spray axis under the effect of the vortices. The vortices are induced by the entrainment of the surrounding gas and act as the driving forces that push the spray plumes towards the axis at the

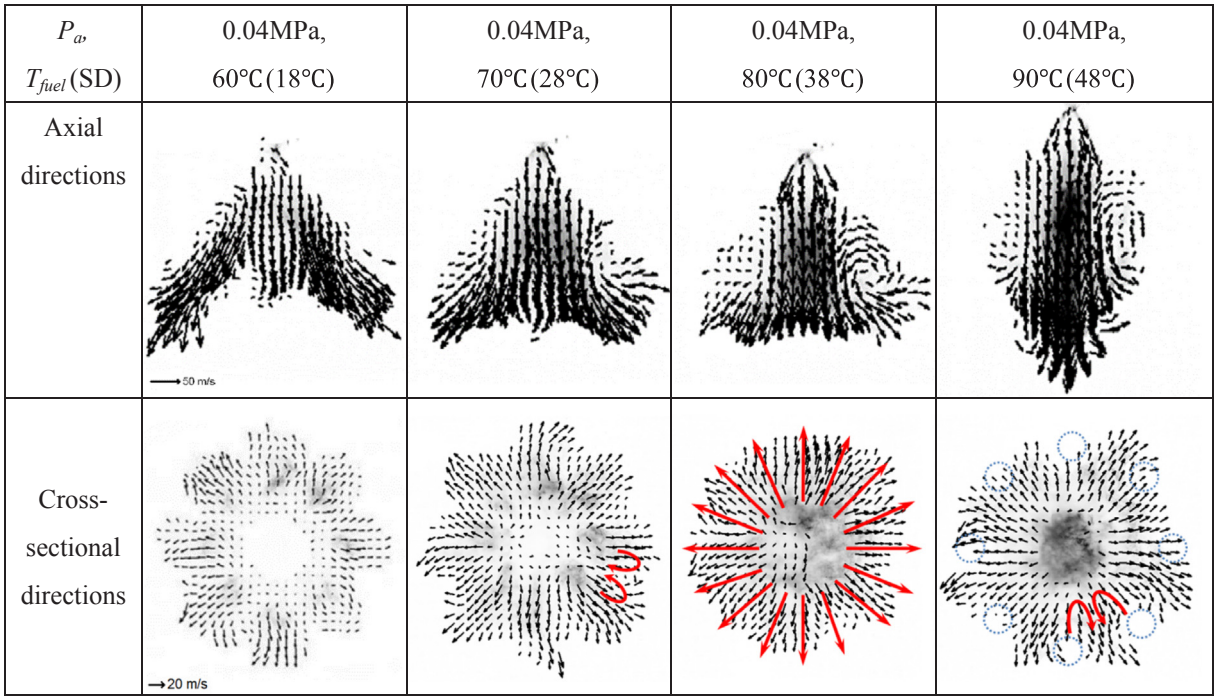

Fig. 9. Velocity vector field in the axial and cross-sectional directions under various superheated conditions (Fuel: *n*-hexane, P_{inj} = 5 MPa, t_{ASOI} = 1 ms, P_a = 40 kPa, Distance of cross section to injector tip: 30 mm. As the SD increases, the velocity of the spray in the axial direction increases due to the plume interactions and enhancement of the vortex strength) [21,80,81].

same time. The high velocity in the center brings the pressure in the centerline below ambient, which induces flow into the center region thus indirectly verifying the correctness of the collapse mechanism shown in Fig. 5. At high SD conditions (SD = 38 ℃ and 48 ℃), the two vortices grow much bigger and stronger and move closer to the spray axis. This vortex motion results in dramatically increased velocity along the injector axis and forms an accelerating spray tip along the axis. Those vortexes push spray towards the injector centerline and form the collapsed structure. The vortex strength can be calculated using Eqs. (8) and (9), as follows:

$$D = \begin{bmatrix} \frac{\partial v_x}{\partial x} & \frac{\partial v_x}{\partial y} \\ \frac{\partial v_y}{\partial x} & \frac{\partial v_y}{\partial y} \end{bmatrix} = \begin{bmatrix} E_{xx} & E_{xy} \\ E_{yx} & E_{yy} \end{bmatrix} \tag{8}$$

$$\text{Vortex strength} = \max\{0, -(E_{xy}E_{yx} - (E_{xx}E_{yy}))/2 + (E_{xx}^2/E_{yy}^2)/4\} \tag{9}$$

The large vortices near the spray front are considered a significant feature of the flash boiling spray flow fields. The vortex core (i.e., the center of the vortex) can be determined by calculating the maximum vortex strength. It was found that as the SD increases, the vortex core moves towards the injector axis in the radial direction and downwards in the axial direction.

The bottom row of Fig. 9 shows the spray particle velocity in the cross-sectional directions. At lower superheat conditions (an SD of 18 ℃), the magnitude of the spray particle velocity is small, and no obvious interaction between the expanded spray plumes can be observed. Upon increasing the SD to 28 ℃, the spray plumes significantly expand and parts of the spray plumes start to interact and form a mixing zone. Small vortices are present within this mixing zone owing to the shear force caused by the differences in velocity. Upon increasing the SD to 38 ℃, the mixing layer between the plumes further develops, and the local velocities increase to a magnitude comparable to the plume main stream. The velocity field along the ring structure appears uniform and no visible vortex exits in the flow-field. At the highest superheat condition (an SD of 48 ℃), velocity peaks appear in the region between the adjacent plumes, and the velocity vectors are bent toward the peaks.

Zhang et al. [51] studied the evaporation and temperature distribution of flash boiling sprays by using the LIEF technique. The upper row of Fig. 10 shows the distribution of the liquid temperature under different SDs. The method for calculating the temperature distribution is described in Section 3.2. Relatively uniform temperature distributions are observed under the subcooled condition. In a transitional condition (i.e., 0.3 < P_a/P_s < 1), the liquid temperature near the centerline is much higher than that of the outer zone. Under flare flash boiling conditions (i.e., P_a/P_s < 0.3), the spray collapses into a solid structure with two particularly high temperature regions: one along the spray centerline, and the other in the outer vortex region. As soon as the liquid fuel leaves the nozzle, it is vaporized and immediately transported toward the spray centerline by the low-pressure region to form a "gas jet" structure. The vortex region likely forms due to the limited heat transfer rate caused by the strong vortex motion. The bottom row of Fig. 9 shows the distribution of vapor concentration under different SDs. When the ambient-to-saturation pressure is reduced to 0.33, the vapor components of the spray plumes become wider and more vapor is present. When the fuel is superheated further (0.16 of P_a/P_s), a "jet-like" vapor structure forms and the entire vapor collapses into the centerline of the injector axis to form a narrow and highly concentrated vapor area.

Aleiferis et al. [15] studied the spray development near the nozzle exit and atomization characteristics under hot fuel conditions. Images of the left-hand-side plume, as shown in Fig. 11, were captured using

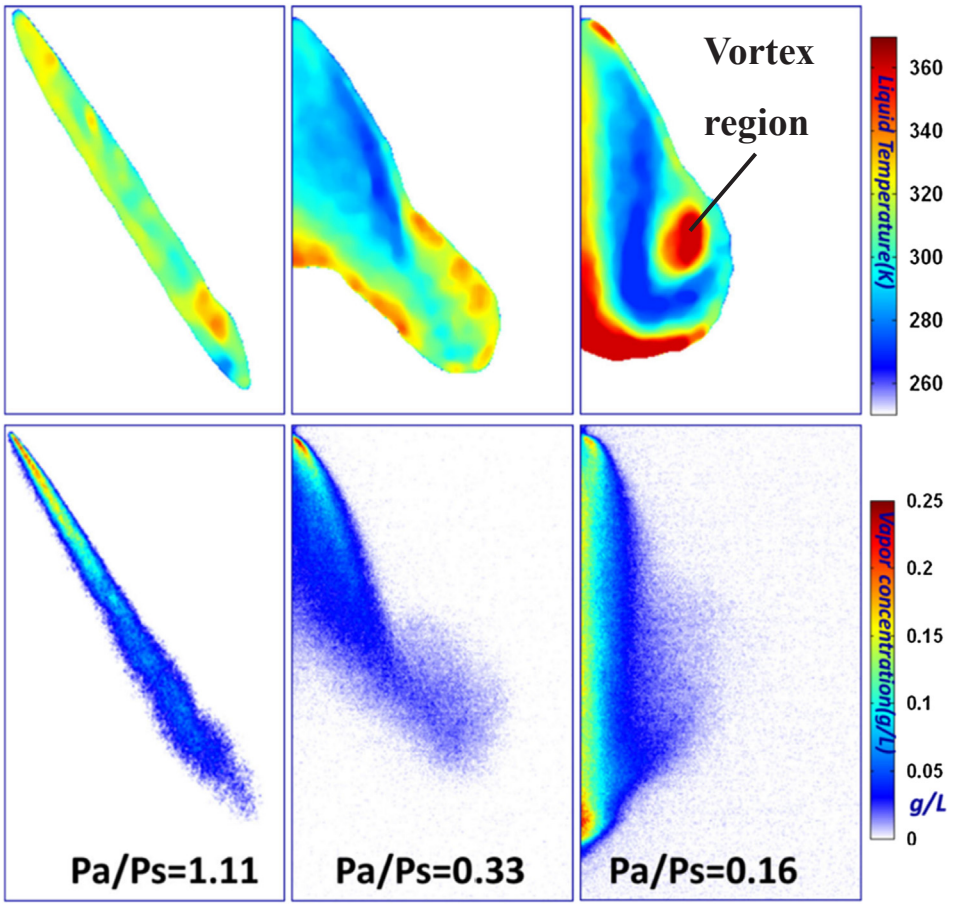

Fig. 10. Distribution of the liquid temperature and vapor concentration under different SDs. (T_{fuel} = 348 K, P_{inj} = 10 MPa, P_a = 1.4 MPa/40 MPa/20 MPa (left/middle/right), t_{ASOI} = 0.7 ms, Injection duration: 1.2 ms. As the SD increases, the liquid temperature near the centerline and in the vortex region is much higher, and the concentrated vapor area moves to the center axis of the spray) [51].

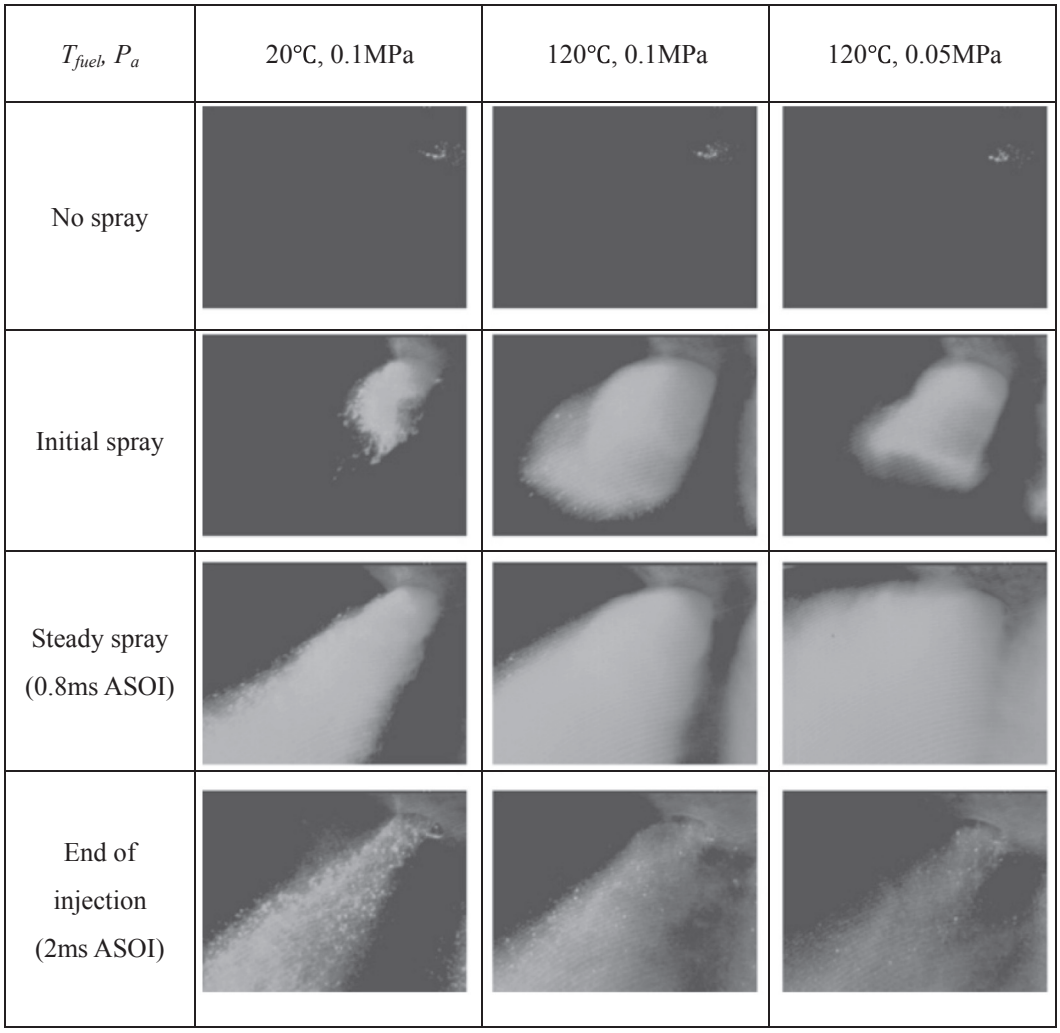

Fig. 11. Left-hand-side plume development of gasoline under different fuel temperatures and ambient pressures (P_{inj} = 15 MPa, Injection duration: 1.5 ms. As the SD increases, the number of large droplets reduces and the boundary of the spray is no longer clear due to improved atomization and evaporation) [15].

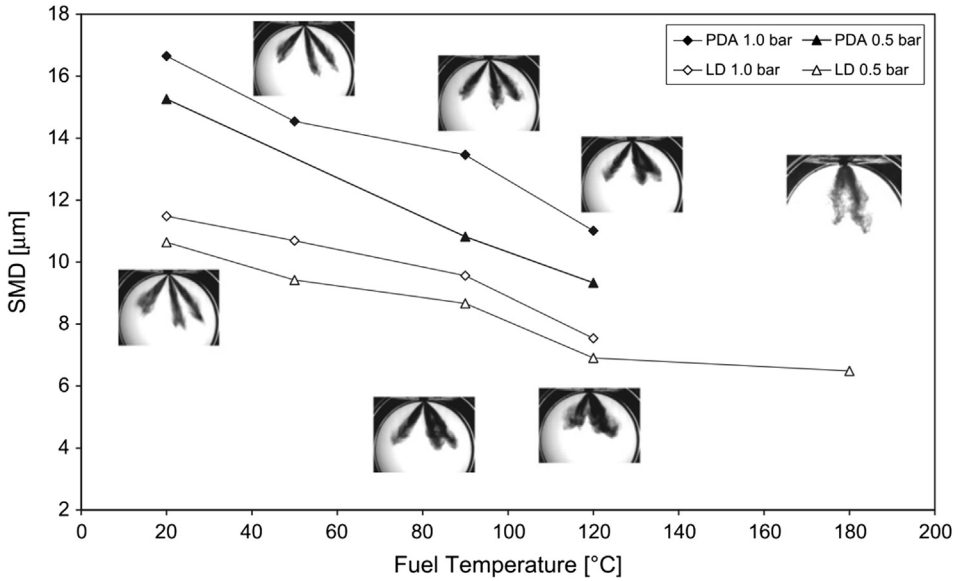

Fig. 12. The SMD of gasoline under different fuel temperatures and ambient pressures (P_{inj} = 15 MPa, Injection duration: 1.5 ms, PDA test point: 25 mm from injector tip, LD test point: 25 mm from injector tip. As the fuel temperature increases, the droplet diameter decreases) [15].

laser sheet pulsed illumination. The initial spray at nominally ambient conditions (T_{fuel} = 20 °C, P_a = 0.1 MPa) clearly showed discernable individual liquid ligaments and droplets around the edge of the spray. In a steady state condition, at 0.8 ms after start of injection (ASOI), the spray plume displayed a clear boundary and plume surface. However, at the end of the injection event (2 ms ASOI), the spray plume showed a number of larger droplets associated with reduced break-up energy as the needle valve closed. At a fuel temperature of 120 °C and 0.5 MPa ambient pressure, the spray boundaries and leading edge were no longer clear, and there was a gradual reduction in the spray brightness due to evaporation. In a steady state condition (at 0.8 ms ASOI), the spray plume displayed a wider boundary due to the rapid breakage of bubbles inside the spray. At the end of the injection event, large droplets were observed suspended in a blurry mist in the image (at 2 ms ASOI). This is attributed to the various components that comprise gasoline. The low-boiling components quickly evaporate, atomize, and exit the nozzle to form a blurry mist, while the high-boiling components remain in droplet form.

Aleiferis et al. [15] also studied the effect of fuel temperature on the atomization characteristics of gasoline spray as shown in Fig. 12. The droplet diameter (SMD) was measured by both phase Doppler (PDA) and laser diffraction (LD) techniques. The PDA results were acquired at a point source 25 mm along the z-axis below the injector nozzle in the center of the middle plume. The LD results that were measured at a point source 30 mm along the z-axis below the injector nozzle in the center of the right plume. The measured SMD steadily decreased with an increase in the fuel temperature, and a sharp reduction in droplet size was observed as the spray collapse condition was approached. This rapid reduction in the measured droplet size was attributed to the increase in the rate of break-up and evaporation once the boiling point of the fuel was exceeded. In addition, the reduction trend as the fuel temperature increased became more pronounced at 25 mm along the z-axis below the injector nozzle than at 30 mm.

Through a comparative study of the velocity field, temperature field, vapor concentration field and droplet diameter, shown in Figs. 9–11, we can further understand the mechanism of the spray collapse. Under high superheat conditions, the spray is immediately vaporized after gasoline is injected from the nozzle. The expanded plumes make contact with each other and form a closed region. As the vaporized spray among the plumes cannot exit the closed region, it is transported toward the central axis. This results in a high velocity along the central axis and the formation of a central low pressure zone. At the same time, the diameter of the droplets decreases continuously due to a higher rate of break-up and evaporation. Once the droplet size falls below a certain critical diameter, which is possibly related to the liquid density, their momentum along the spray plume trajectory is diminished to the extent that they can be pushed into the low-pressure region in the center of the spray. The pressure difference between the outside and center of spray causes the sides of the spray downstream to form vortices. The center of the vortices move toward the center of the spray as the degree of superheating increases, resulting in the spray collapse.

Zeng et al. [46] used the spray tip penetration and spray plume width as the criteria for determining distinct spray regions and studied the structural transformation of the spray and vaporization processes by using a GDI multi-hole injector. Three regions were identified to describe the changes to the spray structure, as shown in Fig. 13. These regions are the non-flash boiling region, transitional flash-boiling region, and flare flash boiling region. The boundary between the non-flash boiling region and transition region was identified as the flash boiling point, and the boundary between the transition region and flash boiling region was identified as the collapse point. Representative images of the spray in each region are shown in the upper portion of the figure, and it can be clearly seen that the spray morphology changed drastically due to the dramatic phase changes in the transition region. The spray characteristics, including the spray tip penetration, spray plume width, and vapor quantity, are presented in the lower portion of the figure.

In non-flash boiling conditions (P_a/P_s > 1), the spray characteristics shown in Fig. 13 are not largely dependent on the ambient-to-saturation pressure ratio, but are mainly determined by the fuel properties and injection conditions. The spray breakup is primarily caused by the forces that act on the surface of the liquid jet, such as the inertia force, viscous force and aerodynamic drag, as mentioned in Section 1.

Under flash-boiling conditions, vapor bubbles start to form within liquid. The spray breakup is mainly determined by the breakup of the bubbles inside the liquid jet, which has significant influence on the spray characteristics. As shown in the figure, larger vapor quantities are generated with decreasing ambient-to-saturation pressure ratio, owing to the increased vapor formed within the superheated liquid and the increased evaporation on the liquid droplet surface. In addition, the vapor quantity in the flare flash boiling region is significantly larger compared to the transitional flash boiling region. This is because the spray fully collapsed in the flare flash boiling region, and the vapor moved along the centerline of the collapsed spray at high speed, which further promoted evaporation of the spray [21].

In the transitional flash boiling region (0.3 < P_a/P_s < 1), the structure of the flash boiling spray is different from that of the non-flash boiling spray due to difference in the breakup mechanism. In this region, vapor bubbles form and grow as the local pressure drops below the fuel's saturation pressure. The vapor bubbles enhance the breakup process and lead to improved atomization of the spray, which is consistent with the results in Fig. 12 which show that the SMD decreased with a decreasing ambient-to-saturation pressure ratio (i.e., increasing SD). In addition, as the ambient-to-saturation pressure ratio decreased, the spray tip penetration decreased and the spray-plume width increased. There are two likely reasons that explain this change. First, the smaller droplets increase the effect of the vapor and air drag forces, leading to the transformation of the spray momentum from the axial direction to the radial direction [52]. Second, the spray loses its designed direction because of the enhanced plume interactions and breakup of the bubbles in the flash boiling spray.

However, in the flare flash-boiling region (P_a/P_s < 0.3), the spray tip penetration increased and the spray plume width decreased with a decrease in the ambient-to-saturation pressure ratio. This was caused by the collapse of the spray in the flare flash region, as mentioned previously.

Different from Zeng's investigations, Du et al. [53,54] used optical

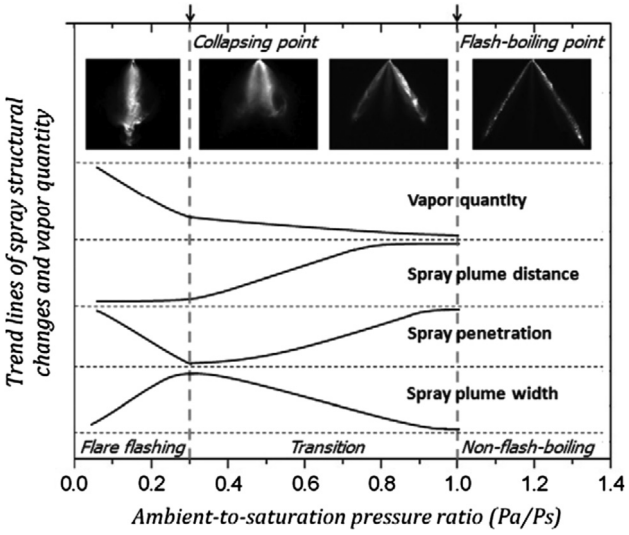

Fig. 13. Macroscopic spray structure and vapor quantity for flash-boiling sprays (P_{inj} = 5 MPa, Injection duration: 1.2 ms. The "flash boiling point" and "collapsing point" is the turning point at which the spray characteristics and evaporation characteristics change sharply) [46].

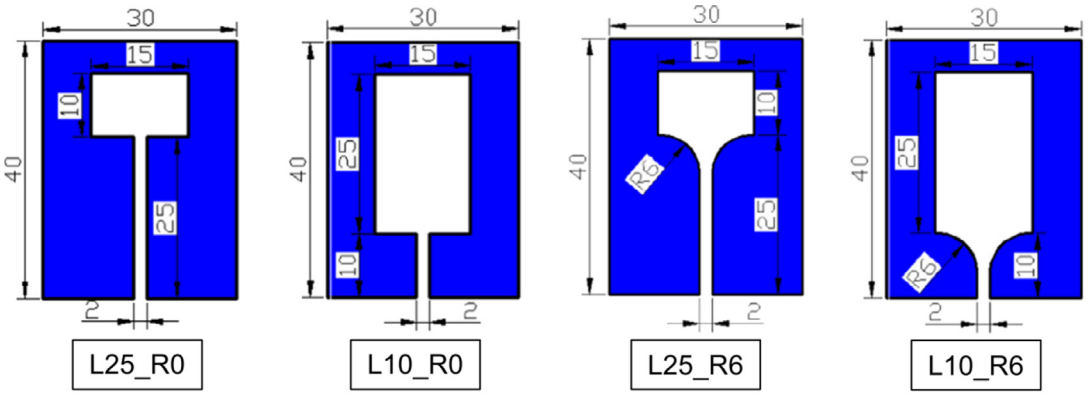

(a) Test slits and corresponding nomenclature (L=slit length, R=inlet corner radius).

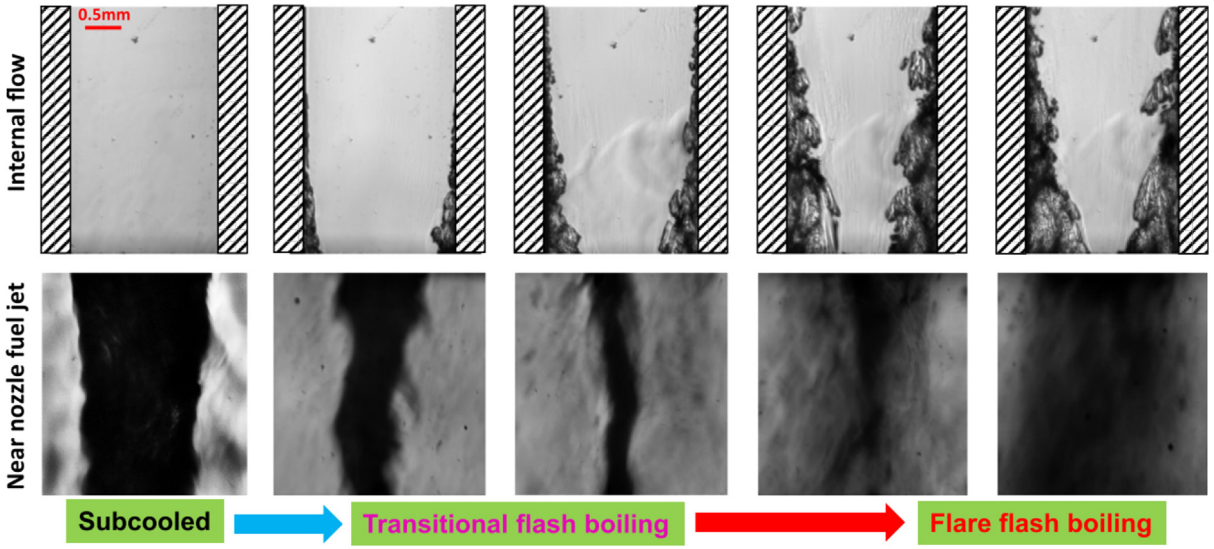

(b) Internal flow and near-nozzle fuel jet of nozzle L25_R0 under various conditions (P_{inj}= 0.6 MPa)

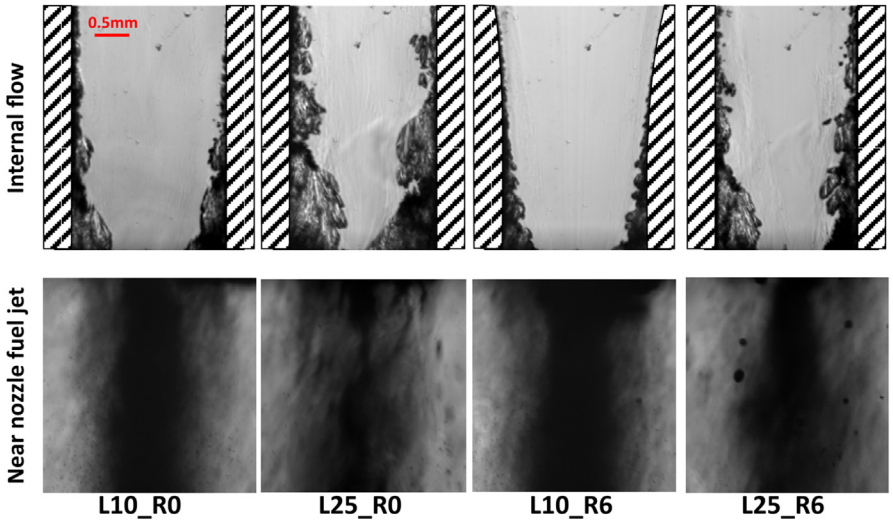

(c) Internal flow and near-nozzle fuel jet of various nozzles under flare flash boiling (T_{fuel}=71°C, P_a=0.07 MPa, P_{inj}= 0.6 MPa)

Fig. 14. Internal flow and near-nozzle fuel jet of different nozzles (As the SD increases, the number of bubbles inside the nozzle increases resulting in a more uniform spray distribution. The number of bubbles increases with a longer nozzle length and sharper nozzle inlet corner) [57].

thickness as the criteria for determining distinct spray regions by using a wide angle multi-hole GDI injector. The optical thickness was based on the entire spray area, which was less sensitive to threshold selection and shot to shot variations. Because the injector had a wide angle, the interaction between the spray plumes was complex. As a result, the starting point of the transition region and flare flash boiling region shifted to a low P_a/P_s compared to the investigations in Zeng's study.

Generally, the SD or P_a/P_s is considered to be one of the main parameters for determining the characteristics of the flash boiling spray. As the SD increases, the spray displays better evaporation and atomization characteristics. In the transition flash boiling region, the plume widens and the plumes begin to interact. The spray tip penetration decreases slightly while the spray width increases slightly. As the spray moves from the transition flash boiling region to the flare flash boiling region, the spray plumes start to move to the spray center. The spray tip penetration increases, but the spray width decreases because the direction of the spray changes to the vertical direction. This is caused by the interaction of the plumes and the driving force of the air outside the spray.

4.2. *Effect of injector configuration on the characteristics of the flash boiling spray*

The injector configuration including the hole length, diameter, number, and angle between the holes, is another key factor affecting the in-nozzle flow of fuel and the collapse process of the spray under flash boiling conditions; thus, affecting the spray behavior outside the nozzle [55,56].

Because it is difficult to observe the flow inside the injector, a transparent nozzle is typically used to simulate the injector nozzle and generate a visualization of the inside of the nozzle. Wu et al. [57] studied the internal flow and liquid jet near the nozzle under no-flash boiling and flash boiling conditions using designed 2D transparent slit nozzles (L10_R0, L25_R0, L10_R6, L25_R6) with different lengths and inlet radii as shown in Fig. 14(a). Fig. 14(b) shows the internal flow and fuel jet near nozzle L25_R0 under various conditions. Observation of the internal flow of fuel revealed that some bubbles were generated along the nozzle wall under flash boiling conditions, and the number of bubbles increased with an increase in the SD. Through observation of the fuel jet near the nozzle, a narrower liquid core with more droplets and ligaments was noted near the nozzle exit under flash boiling conditions, which was considered to be a result of the enhanced atomization of the fuel jet. However, the spray width is not clear in this figure,

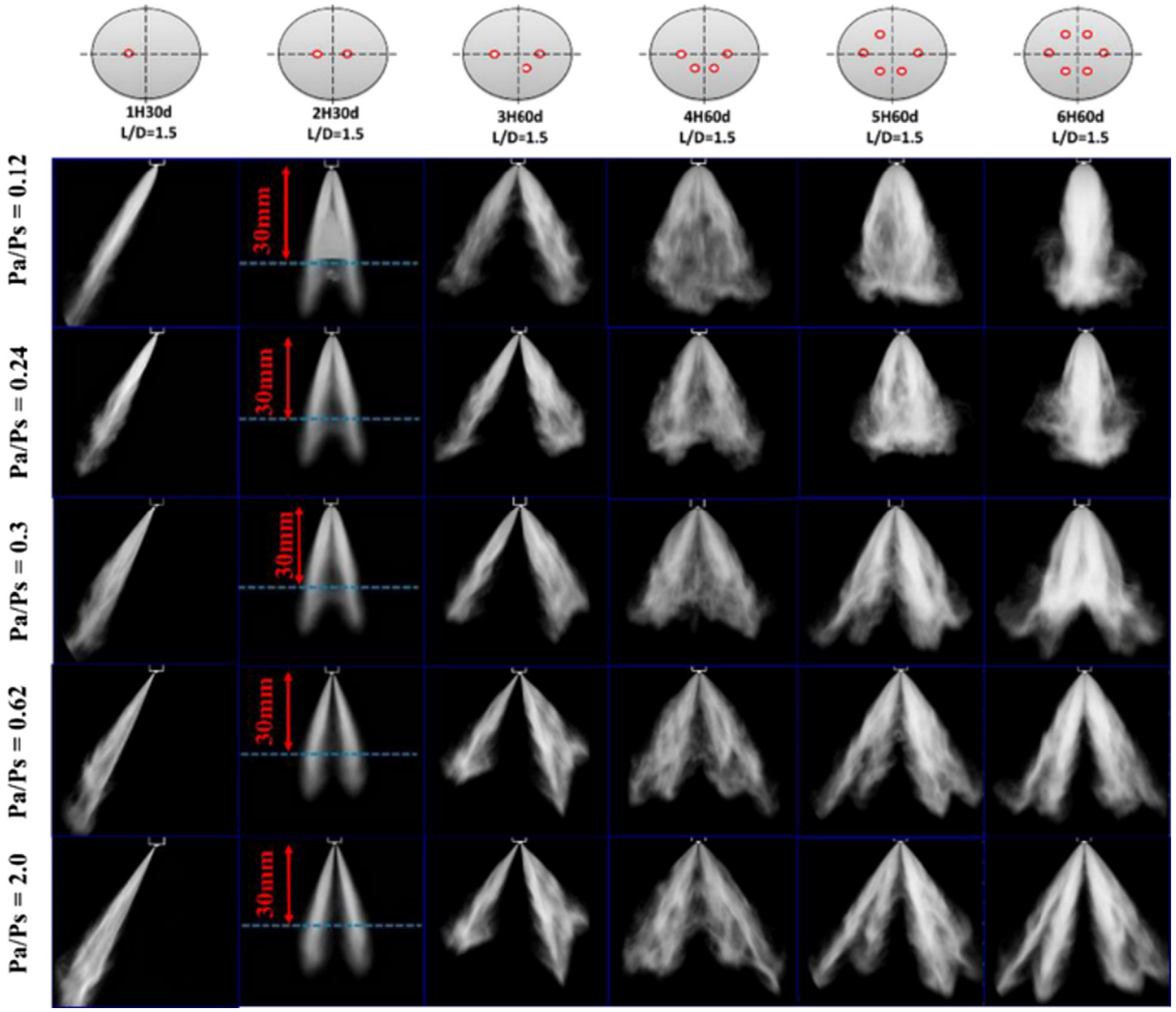

(a) Fuel spray structure transition in the vertical plane (P_{inj}=15 MPa, t_{ASOI} = 0.8 ms)

Fig. 15. Fuel spray structure transition under various SD (The number of holes and hole-to-hole angle dominate the plume separation and plume-to-plume interactions) [60].

because only a portion of the spray is shown in the images. In Yang's investigations [58], the spray width of a transparent 2-D nozzle was increased by increasing the fuel temperature, which was consistent with the results of a single hole injector [43,59]. Fig. 14(c) shows the internal flow and fuel jet near the nozzle of various nozzles at flare flash boiling conditions. The longer nozzles (L25_R0 and L25_R6) formed more bubbles due to the extra time available for bubbles to grow inside the nozzle. Thus, fuel jet disintegration was promoted. In addition, the nozzles with sharp inlet corners (L10_R0 and L25_R0) promoted the generation of more bubbles inside the nozzle compared with the nozzles with round inlet corners (L10_R6 and L25_R6). It was thought that cavitation might occur at the nozzle entrance, which would promote the nucleation process of flash boiling bubbles. Furthermore, the nozzles with sharp inlet corners demonstrated a larger reduction in velocity, which resulted in slightly more time for bubbles to grow inside the nozzle. As a result, more bubbles were observed along the wall of the nozzles with sharp inlet corners and a more uniform spray distribution was observed near the nozzle. In particular, nozzle L25_R0 had the most bubbles inside it, and the most uniform spray distribution near the nozzle due to its length and sharp inlet corner.

Fig. 15 shows the various nozzle configurations of multi-hole injectors ranging from one-hole to six-hole, with different spray exit angles [60]. In the figure, "H" is the number of injector holes, "d" is the angle between the spray exit and vertical plane, and "L/D" is the ratio of the nozzle length and nozzle diameter. For single hole injectors, the macroscopic spray structures under different SDs are quite similar. However, a slight increase in the spray width near the nozzle exit can be seen as the SD increased owing to evaporation and boiling of the fuel both inside and outside the nozzle. The same conclusions have been found in other investigations [34,43,61]. For the 2-hole injector, as the SD continued to increase, the width of the spray plumes increased and the interval between the two plumes became narrower until it disappeared. Finally, the clear separate structure of the two plumes could no longer be discerned owing to the intense gas phase interaction destroying the direction in which the plumes were designed. In addition, Xu et al. [62] found that a secondary plume was generated in the spray central region of two primary plumes under some flash-boiling conditions by using a laser sheet, and that this behavior had a clear relation to the degree of superheating. For the 3-hole injector, the structure of the left plume under different superheated conditions did not change significantly, and behaved similarly to the plume of the single hole injector. However, the adjacent plumes in the right side exhibited more

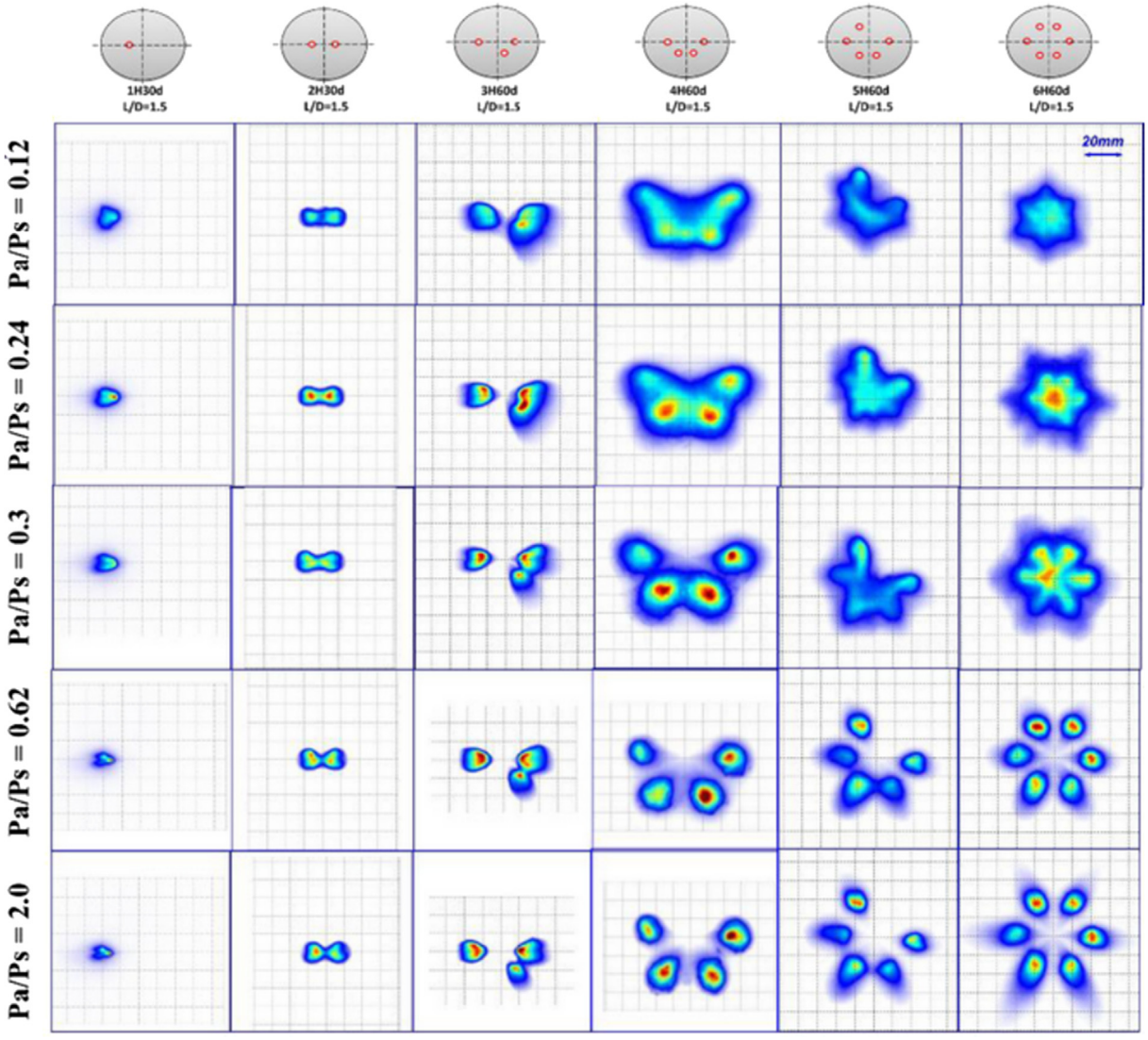

(b) Fuel spray structure transition in the cross-sectional dirction (Distance from cross section to injector tip: 30 mm, t_{ASOI} = 0.8 ms)

Fig. 15. (*continued*)

collapsing behavior owing to increased plume-to-plume interaction, which was a result of an increase in the SD. For the 6-hole injector, in the vertical direction, a spray tip vortex and partial collapse appeared in the transition region and the plume completely collapsed to form a single one central spray as the SD increased in the flare flashing region. In the horizontal direction, the interaction between the spray plumes strengthened and formed a closed circular pattern as the SD increased in the transition region. Then, in the flare flashing region, the spray plume moved to the central part of the spray along with an enormous change in the fuel distribution, which was considered to be a complete collapse. In addition, the spray plumes became larger and their patterns in the cross-section became uniform the SD increased for all the injectors tested.

Injector configuration is considered to be another parameter that affects the characteristics of the flash boiling spray. A longer nozzle led to more bubble formation owing to a longer available time for bubbles to grow inside the nozzle. Thus, fuel jet disintegration was promoted. As a result, a more uniform spray distribution was observed near the nozzle. In addition, compared with a nozzle with a round inlet corner, a nozzle with a sharp inlet corner promoted the generation of internal bubbles. A comparison of injectors with different hole numbers revealed that the injectors with fewer holes showed stronger resistance to spray collapse, than the injectors with more holes. For symmetric nozzle configurations with more holes, the interactions among the plumes are further promoted under flash boiling conditions, which leads to spray collapse.

5. Numerical study of flash boiling

To simulate the superheated liquids injected from the injector, a numerical study should include modeling for the phenomenon of vapor nucleation, which occurs in the injector nozzle and effervescent atomization, which takes place right after the nozzle exit. In addition, the flash boiling model must be able to predict the secondary breakup caused by the bursting of bubbles inside the droplet by aerodynamic breakup. Thus, the modeling of flash boiling is classified into three parts; nucleation, bubble growth and evaporation. The Eulerian-Eulerian and Eulerian-Lagrangian methods are two typical approaches used to numerically simulate fuel spray. The gas phase is calculated using the Eulerian method in both approaches, and the liquid droplets are treated as Eulerian and Lagrangian in the Eulerian-Eulerian and Eulerian-Lagrangian methods, respectively. The analysis domain of the Eulerian-Eulerian method includes the nozzle geometry and spray regime to predict flashing inception inside the nozzle, since nucleation of the vapor phase by the superheated condition occurs from the nozzle. Most spray simulations resort to the Eulerian-Lagrangian method, which has a low computational cost and is suitable for modeling and optimizing sub-models including primary breakup models, the secondary breakup model, and other processes to capture droplet breakup. [63–66].

5.1. Nucleation model

In the Eulerian-Eulerian method, the sink or source term in the governing equation represents the phase change of the liquid and gas fuel provided by the flash boiling models. The homogeneous relaxation model (HRM) calculates the change rate of the vapor fraction by providing a timescale, θ, that reaches the local thermal equilibrium [20,67–69]. The deviation rate of the vapor quality, which refer to the mass fraction of the vapor is defined by Eq. (10):

$$\frac{\mathrm{Dx}}{\mathrm{Dt}} = \frac{\bar{x} - x}{\theta} \tag{10}$$

$$\theta = \theta_0 (\alpha_v + \alpha_{N_2} + \alpha_{O_2})^{-0.54} \left(\frac{|P_{sat} - p|}{p_{crit} - p_{sat}} \right)^{-1.76} \tag{11}$$

where α_v, α_{N_2}, and α_{O_2} are the void fraction of vapor fuel, nitrogen, and oxygen, respectively; and P_{sat}, and p_{crit} are the saturation and critical pressure, respectively. Liquid fuel is as assumed to be incompressible.

The Lagrangian-Eulerian approach, which is another method to simulate liquid fuel injection, adopts the flash boiling model as the initial nozzle boundary conditions. Price et al. [70] discussed the possibility of simulating multi-hole flash boiling spray using various initial droplet diameters, cone angles, and heat transfer coefficients for superheated droplet evaporation. A smaller initial droplet size and wider cone angle leads to a higher correspondence between the simulated and experimental results of the spray in terms of spray collapse, penetration, and SMD in the superheated condition.

Rongshan et al. [66] applied an effervescent atomizer model as the primary breakup model to predict the initial boundary conditions, which include the initial droplet velocity and median diameter. The original velocity of droplet u is calculated using the mass conservation law, fraction, and median diameter, d_0, given by:

$$d_0 = d_{max} e^{-(\theta/\Theta_s)^2} \tag{12}$$

where d_{max} is the maximum droplet diameter that coincides with the effective nozzle area, θ is the cone angle and Θ_s is calculated as the gas mass fraction over the dispersion coefficient. The Taylor Analogy Breakup (TAB) model has been used to simulate the secondary breakup by aerodynamic force. Khan et al. [12] proposed the decomposition of the velocity vector into axial and radial velocities and predicted a high

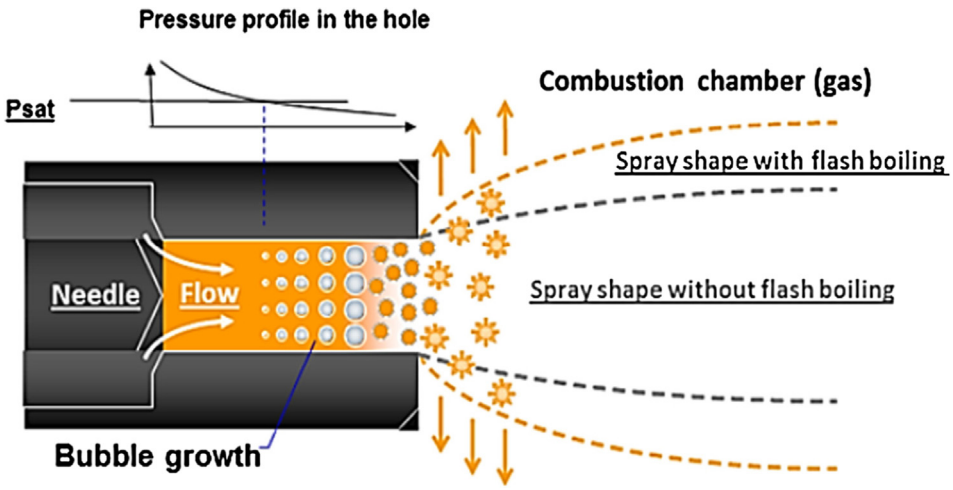

Fig. 16. Schematic of the flash boiling process with bubble explosions and a wider spray cone angle [12].

radial velocity caused by the explosion of bubbles at the nozzle exit. The axial velocity is determined by the mass flow rate from the injector, and the radial velocity is calculated using the ratio of the surface tension force to the average diameter of the droplet. Droplets having high radial velocities and smaller sizes owing to the explosion of bubbles expand the spray plumes radially, resulting in a wider spray cone angle as illustrated in Fig. 16.

The Riznic nucleation model [71,72] was utilized to predict the nucleation site density, bubble departure diameter and bubble departure frequency in the injector nozzle flow under various SDs as disputed by Huang et al. [72] The initial droplet diameter at the nozzle exit, which was reduced by flash-boiling, was calculated by the vapor fuel volume flow, which was determined by bubble parameters. The equation for the diameter reduction factor, R_D, is expressed as follows:

$$R_D = \frac{\dot{V}_l}{\dot{V}_t} = \frac{(\dot{V}_t - \dot{V}_v)}{\dot{V}_t} \tag{13}$$

where $\dot{V}_t$, $\dot{V}_l$ and $\dot{V}_v$ are the total, liquid and vapor fuel volume flow rates in the nozzle respectively. $\dot{V}_v$ is determined by calculating the bubble number, N_n, bubble volume, V_b, and frequency, f,which are functions of the liquid and vapor fuel densities, ρ_l and ρ_v, bubble diameter, D_b, and saturation temperature, T_{sat}, at a given ambient pressure. The equations for $\dot{V}_v$, N_n, and D_b are expressed as follows:

$$\dot{V}_v = N_n V_b f S_n \tag{14}$$

$$N_n = 2.157\frac{1}{D_b^2}\left[\frac{2\sigma T_{sat}}{D_b(T_l - T_{sat})\rho_v H_{vap}}\right]^{-y} e^{-7}(\rho^*)^{-3.1}(1 + 0.0049\rho^*)^{4.1} \tag{15}$$

$$D_b = 2.64e^{-5}\theta\left[\frac{\sigma}{g(\rho_l - \rho_v)}\right]^{0.5}(\rho^*)^{0.9}. \tag{16}$$

Price et al. [71] compared the Riznic and Janet nucleation models, which were designed with a reduction factor using the same equations and the number, diameter, and frequency of bubbles at the nozzle exit using different equations. The Janet nucleation model defined the number and diameter of the bubbles as functions of only the liquid fuel temperature and saturation temperature, and is described as follows:

$$N_{nuc} = 7.937 \times 10^5 \frac{T_l - T_{sat}}{10} \tag{17}$$

$$D_b = max\left(6 \times 10^{-4} exp\left(\frac{T_l - T_{sat}}{45}\right), 1.4 \times 10^{-3}\right). \tag{18}$$

All the numbers included in the above equations are default values. Both the Riznic and Janet nucleation models produce reasonable trends for the initial droplet diameter reduction for various ambient pressure and liquid temperatures. The sensitivity of the diameter reduction factor to the ambient pressure is more substantial in the Janet nucleation model

5.2. Bubble growth and break-up model

In Section 5.1, flash boiling nucleation models were only used to predict the change in nozzle boundary conditions (i.e., the droplet departure diameter, velocity, and frequency) caused by the explosion of bubbles. However, droplets that are injected in superheated conditions are in a thermal non-equilibrium state with the surrounding gas, and the bubbles remain and grow into droplets. Secondary breakup occurs owing to simultaneous aerodynamic force and explosion of the grown bubble.

Bubble growth modeling assumes that the bubbles grow spherically in the droplets, and the Rayleigh–Plesset equation is commonly used to describe the bubble growth process. [11,73–77]. The bubble radius, R, is determined by hydrodynamic forces in accordance with the following:

$$R\ddot{R} + \frac{3}{2}\dot{R}^2 = \frac{1}{\rho}(P_W - P_r) \tag{19}$$

$$P_W = P_V + \left(P_{ro} + \frac{2\sigma}{R_0}\right)\left(\frac{R_0}{R}\right)^{3n} - \frac{2\sigma}{R_0} - \frac{4\mu_l\dot{R}}{R} - \frac{4k\dot{R}}{R^2} \tag{20}$$

where P_r is the pressure around the bubble, ρ is the liquid density, and P_W is the liquid pressure at the bubble surface. The growth of the bubbles has a limit in thin liquid film and after the liquid film reaches the limit state, the droplet breaks up, into smaller droplets. The thickness limit of the liquid film is determined by the liquid viscosity, surface tension, growth rate, and number density of the bubble nuclei.

Zeng and Lee [76] postulated that oscillations along the bubble surfaces and droplets led to the system breakup. The limit of the bubble growth and breakup criterion is given by:

$$BRK(t_b) = \frac{R_{o0}e^{\int_0^t bwdt}}{R_o - R_i} = BRK_{crit} \tag{21}$$

where R_o is the droplet radius, and R_i is the bubble radius. Bubbles burst when the value of the break variable, BRK, is BRK_{crit} which is empirically defined as 5.

Jiro et al. [20] and other researchers [11,74,75,77] determined the limit of bubble growth using the void fraction, ε, of the droplets, which is expressed as follows:

$$\varepsilon = \frac{V_{bubble}}{V_{bubble} + V_{liquid}} \tag{22}$$

where V_{liquid} is the volume of the liquid and V_{bubble} is the volume of the bubbles. The critical void fraction for the criteria of bubble explosion ranges from 0.51 to 0.55, depending on the liquid viscosity and surface tension. After bubble disruption, the parent droplets break into smaller droplets, and the number of child droplets is double the number of bubbles [11,75,77]. The momentum of the parent droplet is conserved and distributed equally to the child droplets.

5.3. Vaporization model

In a subcooled condition, the Lagrangian-Eulerian method assumes that spray evaporation occurs on the droplet surface, where the heat transfer between the liquid fuel and ambient gas and the liquid-vapor equilibrium is estimated by evaporation models. With droplets containing vapor fuel bubbles in a superheated condition, vaporization of the liquid fuel is the summation of the subcooled evaporation to the surrounding environment by heat transfer and flash boiling vaporization by superheating.

Price et al. [70,71] described the rate of evaporation of the superheated droplet, $\frac{dM_{sh}}{dt}$, in terms of the difference between the instantaneous droplet temperature and boiling temperature, $T_d - T_b$, latent heat of the fuel, H_v, and a heat transfer coefficient, α, as given in Eq. (23).

$$\frac{dM_{sh}}{dt} = \frac{A\alpha(T_d - T_b)}{H_V} \tag{23}$$

The heat transfer coefficient α differs according to the fuel type and is expressed as an empirical function derived from experimental investigations. This vaporization model for flash boiling simulates external flash boiling in which the fuel vapor from the superheated fuel and evaporation form a vapor film surrounding the droplet. Flash boiling increases the mass transfer rate and lead to an increase in heat transfer from the addition of heat from the phase-change mass transfer.

Vaporization during bubble growth is modeled by the volume change and number of bubbles, N, [73] and the vaporization model is expressed as follows:

$$dM_{ch} = \rho \bullet \frac{4}{3}\pi \sum N(R^3 - R_0^3) \tag{24}$$

where dM_{ch} is the evaporated fuel mass, and R and R_0 are the current and previous radius in each time step, respectively. The heat required for evaporation by bubble growth comes from the liquid film and is calculated as the product of the evaporated fuel mass and the latent heat.

Ra and Reitz [78] estimated the fuel vaporization rate on the droplet surface in superheated conditions using an energy balance between the heat transfer from the bubble to the liquid film, heat transfer from the surrounding air to the droplet surface and heat absorption by the fuel vaporization. The energy balance for the vaporization is calculated using the following equation:

$$\dot{m}L(T_b) = (h_{i,eff,s} + \alpha_{sh})\Delta T + \frac{a\bar{C}_p\dot{m}}{\exp\left[\frac{2r_0\bar{C}_p\dot{m}}{\lambda Nu} - \frac{[C_A](y_{F,sur}-1)}{\lambda}\frac{sh}{Nu}\right]-1}(T_{sur}-T_b) \quad (25)$$

where $\dot{m}$ is the vaporization mass rate, and α_{sh} is the heat transfer enhancement caused by the superheated effects and which varies with the difference between the droplet temperature and saturation temperature.

5.4. Application of numerical models

Using numerical models (i.e., computational fluid dynamics (CFD) codes) is a simple and low-cost method to predict the development of flash sprays for GDI injectors. CFD codes are often used to study the temperature field [68], pressure field [68,69], velocity field [12,69,72], concentration distribution [12,68,70,72], and particle size distribution [70] inside and near the nozzle to gain a deep understanding of the flash boiling process and achieve a more efficient optimization design of the injector.

Guo et al. [68] studied an n-hexane flash boiling spray that was numerically discharged from a single-hole GDI injector. Fig. 17(a) shows the vapor phase mass fraction distribution of the spray at an ambient pressure of 0.02 MPa. Under superheated conditions, a large amount of vapor is generated along the surface of the step hole, leading to the onset of internal flash boiling. In addition, a liquid core can be seen inside the fuel jet, and the length of the liquid core decreases with an increase in the SD due to enhanced evaporation. Fig. 17(b) shows the vapor fraction along the nozzle axis. Generally, the mass fraction of the vapor increases with an increase in the SD. Under superheated conditions, the mass fraction of the vapor phase increases along the nozzle axis. The onset of expansion is defined as corresponding to the position at which the velocity significantly increases. The vapor fraction undergoes a period of rapid increase after the onset of expansion, owing to the evaporation that is promoted by the rapid increase in spray velocity.

Fig. 18(a) shows the pressure distribution of the spray inside and near the nozzle at an ambient pressure of 0.02 MPa. Under subcooled conditions (i.e., a temperature of 30 °C), the pressure is sharply reduced to below ambient pressure along the surface of the step hole, and the

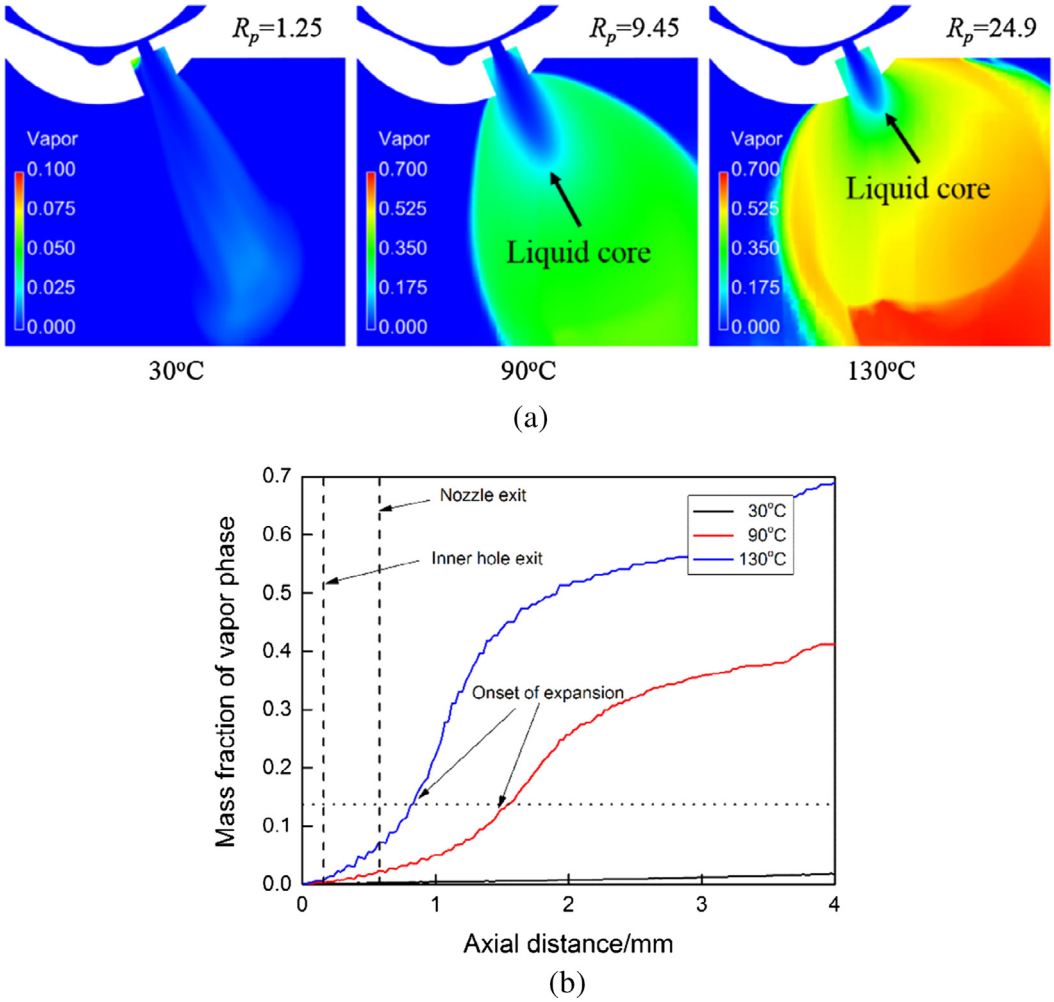

Fig. 17. Mass fraction distribution of the vapor phase (a) and mass fraction along the nozzle axis at different fuel temperatures (b) (Fuel: *n*-hexane, P_{inj} = 10 MPa, P_a = 20 KPa. Considerable vaporization starts at the counter bore and the mass fraction of the vapor phase increases as the axial distance increases) [68].

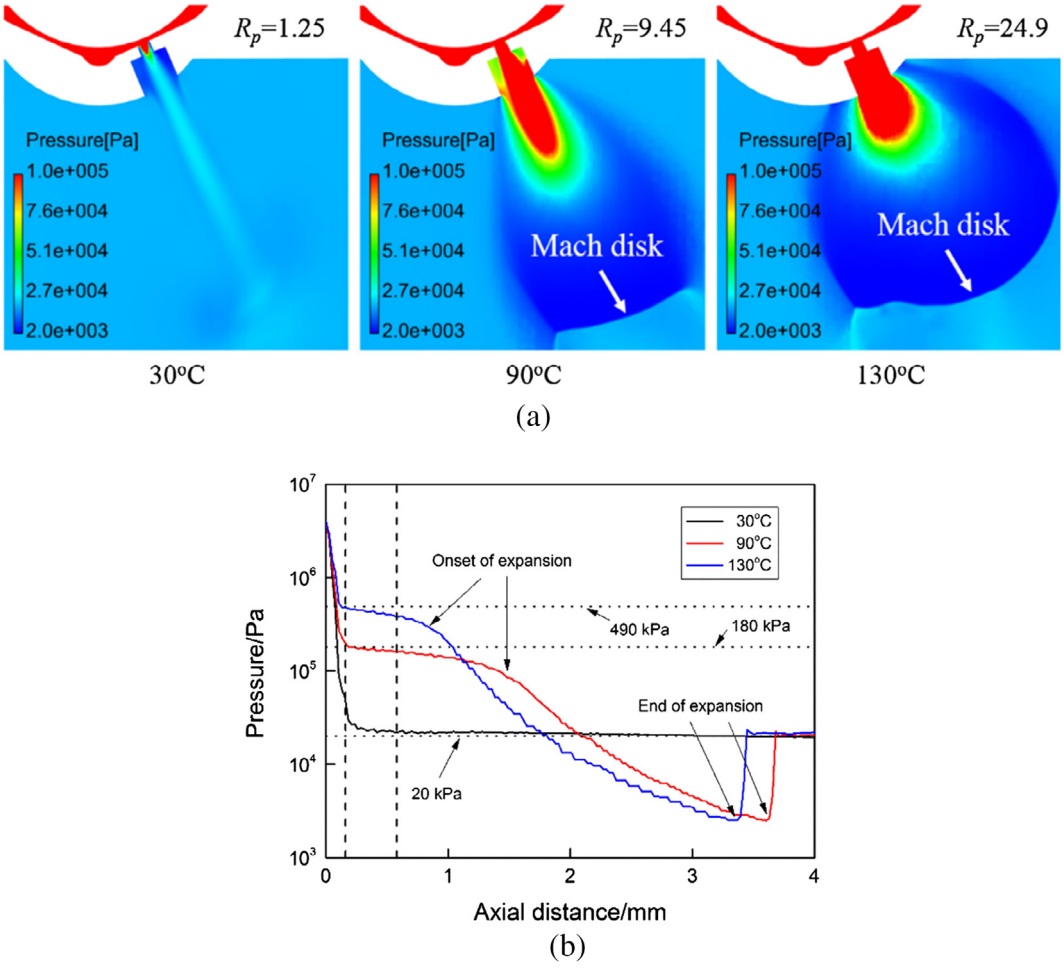

Fig. 18. Pressure distribution of the vapor phase (a) and pressure along the nozzle axis at different fuel temperatures (b) (Fuel: *n*-hexane, P_{inj} = 10 MPa, P_a = 20 KPa. A low pressure region occurs downstream the liquid core and volume of the low-pressure region increases with an increase in SD under superheated conditions) [68].

pressure increased to near ambient pressure after injection from the nozzle. Under superheated conditions, the pressure in the liquid core region was especially high. Downstream of the liquid core, there was a low-pressure region that was lower than the ambient pressure. The volume of the low-pressure region increased with an increase in fuel temperature. The formation of the low-pressure region downstream of the liquid core could be used to explain the spray collapse of the multi-hole injector. Fig. 18(b) shows the pressure of the spray along the nozzle axis at an ambient pressure of 0.02 MPa. At a fuel temperature of 30 °C, the pressure dropped sharply in the nozzle owing to acceleration of the flow as fuel entered the nozzle from the valve body, and then remained close to the ambient pressure. Under superheated conditions (i.e., fuel temperatures of 90 °C and 130 °C), the decreasing trend halted as the pressure reached the saturation pressures of *n*-hexane (180 kPa at 90 °C and 490 kPa at 130 °C). Once the pressure became lower than the saturation pressure, the decreasing trend slowed down owing to the combined effect of evaporation and the step hole. The step hole restricted expansion of the plumes, which enabled the pressure to remain at a level higher than ambient pressure. After the jet exited the nozzle, the pressure continuously decreased until a low-pressure region was formed. There are two likely reasons that might explain the formation of the low-pressure region in the single hole injector. First, the jet expanded drastically owing to the elimination of the hole size limitation. Under the effect of inertia, the spray expanded some at a pressure lower than the ambient. Second, the vaporized spray moved toward the central axis at high velocity, as explained in Section 4.1, which led to the formation of a low-pressure region. In addition, as the axial distance increased, the pressure increased and ultimately stabilized at ambient pressure, even for different fuel temperatures.

Lacey et al. [38] developed a framework to characterize the behavior of the plume interactions and collapse under different superheated conditions. They hypothesized that severe spray collapse occurred when the plumes from the two holes spaced farthest apart had a diameter at least equal to their spacing. Then the collapse diameter can be calculated as:

Table 3
Injector and operating parameters.

Injector	Nozzle diameter(μm)	Counter-bore diameter (μm)	Drill angle (°)	*Pa/Ps*	CP	Distance between adjacent nozzle(μm)
I8	184	330	30	0.98	0.136	568
I2	224	330	37	0.98	0.146	612
I5	224	350	45	0.98	0.112	662

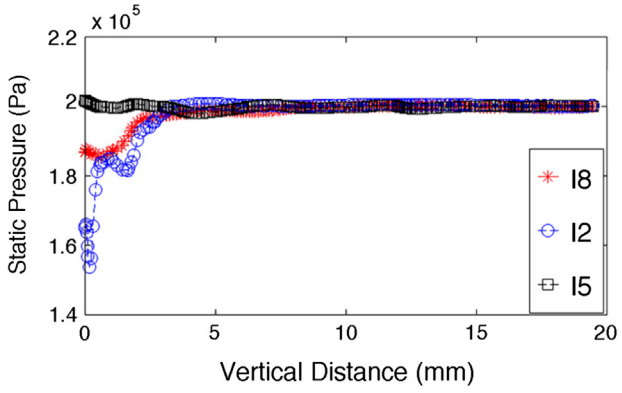

Fig. 19. Centerline static pressure (P_a/P_s = 0.98, P_{inj} = 10 MPa, T_{fuel} = 360 K. A larger CP value led to a larger pressure drop in the centerline static pressure) [69].

$$d_{coll} = \frac{\text{Center-to-center distance between the farthest counter bores}}{\text{Cosine of the drill angle}} \quad (26)$$

The dimensionless parameter is termed the collapse parameter, CP, which is given by:

$$\text{CP} = \frac{diameter\ of\ nozzle\ d}{diameter\ of\ collapse\ d_{coll}} \quad (27)$$

Based on the dimensionless parameter CP, Rachakonda et al. [69] studied the flash boiling spray characteristics of six-hole GDI injectors with different nozzle geometries and ambient to saturation pressures. Table 3 lists the nozzle parameters for each six-hole injector. Fig. 19 shows the centerline static pressure of different injectors. The static pressure was measured along the injector axis and started at the injector tip. In Fig. 19, injector I5 can be seen to have the smallest magnitude of pressure drop, while I2 has the largest magnitude of pressure drop. Table 3 shows that the CP value of I5 is the smallest, while that of I2 is the largest. Therefore, it can be concluded that nozzles with a larger CP value experience a larger drop in centerline static pressure. The magnitude of the pressure drop indicates the strength of the interaction, where a larger drop in the pressure implies a more intense interaction between the two farthest plumes.

The CP is an important dimensionless parameter used to study the effect of nozzle configuration on plume interactions and collapse. A larger CP value leads to a larger pressure drop in the centerline static pressure, which results in enhanced plume interactions and collapse. However, the CP does not consider the nozzle length of the injector, which is also an impotant parameter that reflects the structure of the injector.

6. Conclusions

This review paper presents the flash boiling phenomenon in GDI injectors. The paper provides an overview of the current state of research on this topic, including the theoretical, experimental, and numerical studies relevant to flash boiling processes. The current state can be summarized as follows:

(1) Spray behavior under flash boiling conditions is mainly dependent on two aspects: the degree of superheating that the spray is exposed to, and the nozzle orifice configuration. At a lower degree of superheating, the aerodynamic breakup process enhances liquid fuel dispersion. However, at a higher degree of superheating, interactions among the plumes and collapse of the spray occur, which significantly influence the macroscopic spray characteristics. A longer nozzle leads to the formation of more bubbles in the nozzle because more time is available for the growth of bubbles in the nozzle. Thus, fuel jet disintegration is promoted. In multi-hole injectors, the collapse parameter dominates the plume separation, plume-to-plume interactions and collapse of the spray under flash boiling condition.

(2) Through a comparative study of the velocity field, temperature field, vapor concentration field and droplet diameter, an improved understanding of the collapse mechanism is gained. Under high superheat conditions, the spray was immediately vaporized after the gasoline was injected from the nozzle. The vaporized spray changed the original direction of motion and was transported toward the central axis, resulting in a high velocity along the central axis and formation of a central low-pressure zone. Under the action of the pressure difference between the outside and center of spray, the spray was pushed toward the central axis, resulting in spray collapse.

(3) The effects of vapor formation in the nozzle and bubbles in the droplets under superheated conditions were simulated using flash boiling spray models. Nucleation models predicted that the initial droplet sizes would be reduced by effervescent atomization, and the initial cone angles would be extended by radial velocity, owing to bubble explosion at the nozzle exit. Bubble growth and droplet breakup at the critical void fraction were calculated using bubble growth models. Additional heat transfer from the bubbles and evaporation under superheated conditions were considered in flash boiling spray simulation.

Declaration of Competing Interest

The authors declare that they have no known competing financial interests or personal relationships that could have appeared to influence the work reported in this paper.

Acknowledgements

This research was supported by the Center for Environmentally Friendly Vehicle (CEFV) as a Global-Top Project of the KMOE (Ministry of Environment, Korea) (No. 2019002070001) and by the National Research Foundation of Korea (NRF) grant funded by the Korean government (MSIT, Ministry of Science and ICT) (No. 2019R1A2C1089494).

References

[1] Montanaro A, Allocca L, Meccariello G, Vita AD. Very high-pressure sprays of gasoline from a GDI multi-hole injector. 29th conference on liquid atomization and spray systems. Paris, France. 2019.
[2] Gröger K, Kawaharada N, Klippenstein A, Dinkelacker F. Velocity measurement of high-pressure gasoline direct injections in the primary atomization region on flash boiling conditions. 29th conference on liquid atomization and spray systems. Paris, France. 2019.
[3] Yamaguchi A, Koopmans L, Helmantel A, Karrholm FP, Spray Dahlander P. Characterization of gasoline direct injection sprays under fuel injection pressures up to 150 MPa with different nozzle geometries. SAE International; 2019.
[4] Wang C, Xu H, Herreros JM, Wang J, Cracknell R. Impact of fuel and injection system on particle emissions from a GDI engine. Appl Energy 2014;132:178–91.
[5] Brown RYJL. Sprays formed by flashing liquid jets. AIChE J 1962;8:149–53.
[6] Oza RD, Sinnamon JF. An experimental and analytical study of flash boiling fuel injection. SAE Trans 1983;948–62.
[7] Kim Y, Iwai N, Suto H, Tsuruga T. Improvement of alcohol engine performance by flash boiling injection. 1980.
[8] Reitz RD. A photographic study of flash-boiling atomization. Aerosol Sci Technol 2007;12:561–9.
[9] Zhang G, Grover R, Xu M, Li T, Kuo T-W, He Y. A study of near-field spray structure under superheated conditions of a gasoline fuel spray. 26th annual conference on liquid atomization and spray systems. Portland, Oregon. 2014.
[10] Schmitz I, Ipp W, Leipertz A. Flash boiling effects on the development of gasoline direct-injection engine sprays. SAE technical paper. 2002. p. 1025–32.
[11] Kawano D, Ishii H, Suzuki H, Goto Y, Odaka M, Senda J. Numerical study on flash-boiling spray of multicomponent fuel. Heat Transf Asian Res 2006;35:369–85.
[12] Khan MM, Hélie J, Gorokhovski M, Sheikh NA. Experimental and numerical study of flash boiling in gasoline direct injection sprays. Appl Therm Eng 2017;123:377–89.
[13] Polanco G, Holdø AE, Munday G. General review of flashing jet studies. J Hazard Mater 2010;173:2–18.

[14] Anitescu G, Tavlarides LL, Geana D. Phase transitions and thermal behavior of fuel − diluent mixtures. Energy Fuels 2009;23:3068–77.
[15] Aleiferis PG, van Romunde ZR. An analysis of spray development with iso-octane, n-pentane, gasoline, ethanol and n-butanol from a multi-hole injector under hot fuel conditions. Fuel 2013;105:143–68.
[16] Zeng W, Xu M, Zhang M, Zhang Y, Cleary DJ. Macroscopic characteristics for direct-injection multi-hole sprays using dimensionless analysis. Exp Therm Fluid Sci 2012;40:81–92.
[17] Li Y, Guo H, Fei S, Ma X, Zhang Z, Chen L, et al. An exploration on collapse mechanism of multi-jet flash-boiling sprays. Appl Therm Eng 2018;134:20–8.
[18] Guo H, Ma X, Li Y, Liang S, Wang Z, Xu H, et al. Effect of flash boiling on microscopic and macroscopic spray characteristics in optical GDI engine. Fuel 2017;190:79–89.
[19] Montanaro A, Allocca L. Flash boiling evidences of a multi-hole GDI spray under engine conditions by mie-scattering measurements. SAE International; 2015.
[20] Saha K, Battistoni M, Som S. Modeling of flash boiling phenomenon in internal and near-nozzle flow of fuel injectors. In: Basu S, Agarwal AK, Mukhopadhyay A, Patel C, editors. Droplets and sprays: applications for combustion and propulsion. Singapore: Springer Singapore; 2018. p. 167–81.
[21] Xu M, Zhang Y, Zeng W, Zhang G, Zhang M. Flash boiling easy and better way to generate ideal sprays than the high injection pressure. SAE Int J Fuels Lubr 2013;6:137–48.
[22] Jin Y-I, Lee HJ, Hwang K-Y, Park D-C, Min S. Flashing injection of high temperature hydrocarbon liquid jets. Exp Therm Fluid Sci 2018;90:200–11.
[23] Wang Z, Badawy T, Wang B, Jiang Y, Xu H. Experimental characterization of closely coupled split isooctane sprays under flash boiling conditions. Appl Energy 2017;193:199–209.
[24] Yang J, Dong X, Wu Q, Xu M. Influence of flash boiling spray on the combustion characteristics of a spark-ignition direct-injection optical engine under cold start. Combust Flame 2018;188:66–76.
[25] Huang Y, Hong G. Investigation of the effect of heated ethanol fuel on combustion and emissions of an ethanol direct injection plus gasoline port injection (EDI + GPI) engine. Energy Convers Manage 2016;123:338–47.
[26] Huang Y, Hong G, Huang R. Investigation to charge cooling effect and combustion characteristics of ethanol direct injection in a gasoline port injection engine. Appl Energy 2015;160:244–54.
[27] Liao Y, Lucas D. Computational modelling of flash boiling flows: a literature survey. Int J Heat Mass Transf 2017;111:246–65.
[28] Guo H, Ding H, Li Y, Ma X, Wang Z, Xu H, et al. Comparison of spray collapses at elevated ambient pressure and flash boiling conditions using multi-hole gasoline direct injector. Fuel 2017;199:125–34.
[29] Li S, Zhang Y, Qi W. Quantitative study on the influence of bubble explosion on evaporation characteristics of flash boiling spray using UV-LAS technique. Exp Therm Fluid Sci 2018;98:472–9.
[30] Lamanna G, Kamoun H, Weigand B, Steelant J. Towards a unified treatment of fully flashing sprays. Int J Multiphase Flow 2014;58:168–84.
[31] Mikic BB, Rohsenow WM, Griffith P. On bubble growth rates. Int J Heat Mass Transf 1970;13:657–66.
[32] Sher E, Bar-Kohany T, Rashkovan A. Flash-boiling atomization. Prog Energy Combust Sci 2008;34:417–39.
[33] Li Y, Guo H, Zhou Z, Zhang Z, Ma X, Chen L. Spray morphology transformation of propane, n-hexane and iso-octane under flash-boiling conditions. Fuel 2019;236:677–85.
[34] Guo H, Wang B, Li Y, Xu H, Wu Z. Characterizing external flashing jet from single-hole GDI injector. Int J Heat Mass Transf 2018;121:924–32.
[35] Simões-Moreira JR. Oblique evaporation waves. Shock Waves 2000;10:229–34.
[36] Vieira MM, Simões-Moreira JR. Low-pressure flashing mechanisms in iso-octane liquid jets. J Fluid Mech 2007;572:121–44.
[37] Krämer M, Kull E, Wensing M. Flashboiling-induced targeting changes in gasoline direct injection sprays. Int J Engine Res 2015;17:97–107.
[38] Lacey J, Poursadegh F, Brear MJ, Gordon R, Petersen P, Lakey C, et al. Generalizing the behavior of flash-boiling, plume interaction and spray collapse for multi-hole, direct injection. Fuel 2017;200:345–56.
[39] Huang Y, Huang S, Deng P, Huang R, Hong G. The effect of fuel temperature on the ethanol direct injection spray characteristics of a multi-hole injector. SAE Int J Fuels Lubr 2014;7:792–802.
[40] Li Y, Guo H, Ma X, Qi Y, Wang Z, Xu H, et al. Morphology analysis on multi-jet flash-boiling sprays under wide ambient pressures. Fuel 2018;211:38–47.
[41] Moon S, Bae C, Abo-Serie E, Choi J. Internal and near-nozzle flow of a pressure-swirl atomizer under varied fuel temperature. Atomization Sprays 2007;17:529–50.
[42] Wu S, Yang S, Wooldridge M, Xu M. Experimental study of the spray collapse process of multi-hole gasoline fuel injection at flash boiling conditions. Fuel 2019;242:109–23.
[43] Wu S, Xu M, Hung DLS, Li T, Pan H. Near-nozzle spray and spray collapse characteristics of spark-ignition direct-injection fuel injectors under sub-cooled and superheated conditions. Fuel 2016;183:322–34.
[44] Wang L, Nonavinakere Vinod K, Fang T. Effects of fuels on flash boiling spray from a GDI hollow cone piezoelectric injector. Fuel 2019;257.
[45] Wang L, Wang F, Fang T. Flash boiling hollow cone spray from a GDI injector under different conditions. Int J Multiphase Flow 2019;118:50–63.
[46] Zeng W, Xu M, Zhang G, Zhang Y, Cleary DJ. Atomization and vaporization for flash-boiling multi-hole sprays with alcohol fuels. Fuel 2012;95:287–97.
[47] Settles GS. Shadowgraph Techniques. In: Settles GS, editor. Schlieren and shadowgraph techniques: visualizing phenomena in transparent media. Berlin, Heidelberg: Springer Berlin, Heidelberg; 2001. p. 143–63.
[48] Melton LA. Spectrally separated fluorescence emissions for diesel fuel droplets and vapor. Appl Opt 1983;22:2224–6.
[49] Lavieille P, Lemoine F, Lavergne G, Lebouché M. Evaporating and combusting droplet temperature measurements using two-color laser-induced fluorescence. Exp Fluids 2001;31:45–55.
[50] Wood A, Wigley G, Helie J. Flash boiling sprays produced by a 6-hole GDI injector. 17th international symposium on applications of laser techniques to fluid mechanics. Lisbon, Portugal. 2014. p. 7–10.
[51] Zhang G, Hung DLS, Xu M. Experimental study of flash boiling spray vaporization through quantitative vapor concentration and liquid temperature measurements. Exp Fluids 2014;55:1804.
[52] Vu H, García-Valladares O, Aguilar G. Vapor/liquid phase interaction in flare flashing sprays used in dermatologic cooling. Int J Heat Mass Transf 2008;51:5721–31.
[53] Du J, Mohan Balaji, Sim J, Fang T, Roberts WL. Study of spray collapse phenomenon at flash boiling conditions using simultaneous front and side view imaging. Int J Heat Mass Transf 2020;147.
[54] Du J, Mohan Balaji, Sim J, Chang J, Fang T, Roberts WL. Characterizing flash boiling sprays of E10 gasoline from a high-pressure gasoline multi-hole injector. SAE technical paper. 2019. 2019-01-2249.
[55] Mojtabi M, Chadwick N, Wigley G, Helie J. The effect of flash boiling on breakup and atomisation in GDI sprays. Proceedings of the 22nd European conference on liquid atomization and spray systems ILASS Europe Como Lake, Italy. Como Lake, Italy. 2008.
[56] Mojtabi M, Wigley G, Helie J. The effect of flash boiling on the atomization performance of gasoline direct injection multistream injectors. Atomiz Sprays 2014;24:467–93.
[57] Wu S, Xu M, Hung DLS, Pan H. Effects of nozzle configuration on internal flow and primary jet breakup of flash boiling fuel sprays. Int J Heat Mass Transf 2017;110:730–8.
[58] Yang S, Li X, Hung DLS, Xu M. Characteristics and correlation of nozzle internal flow and jet breakup under flash boiling conditions. Int J Heat Mass Transf 2018;127:959–69.
[59] Yang S, Song Z, Wang T, Yao Z. An experiment study on phenomenon and mechanism of flash boiling spray from a multi-hole gasoline direct injector. Atomiz Sprays 2013;23:379–99.
[60] Aori G, Hung DLS, Zhang M, Zhang G, Li T. Effect of nozzle configuration on macroscopic spray characteristics of multi-hole fuel injectors under superheated conditions. Atomiz Sprays 2016;26:439–62.
[61] Guo H, Li Y, Lu X, Zhou Z, Xu H, Wang Z. Radial expansion of flash boiling jet and its relationship with spray collapse in gasoline direct injection engine. Appl Therm Eng 2019;146:515–25.
[62] Xu Q, Pan H, Gao Y, Li X, Xu M. Investigation of two-hole flash-boiling plume-to-plume interaction and its impact on spray collapse. Int J Heat Mass Transf 2019;138:608–19.
[63] Jiang X, Siamas GA, Jagus K, Karayiannis TG. Physical modelling and advanced simulations of gas–liquid two-phase jet flows in atomization and sprays. Prog Energy Combust Sci 2010;36:131–67.
[64] Yan Y-w, Zhao J-x, Zhang J-z, Liu Y. Large-eddy simulation of two-phase spray combustion for gas turbine combustors. Appl Therm Eng 2008;28:1365–74.
[65] Nieckele AO, Naccache MF, Gomes MSP. Combustion performance of an aluminum melting furnace operating with natural gas and liquid fuel. Appl Therm Eng 2011;31:841–51.
[66] Bi R, Chen C, Li J, Tan X, Xiang S. Research on the CFD numerical simulation of flash boiling atomization. Energy 2018;165:768–81.
[67] Guo H, Li Y, Xu H, Shuai S, Zhang H. Interaction between under-expanded flashing jets: a numerical study. Int J Heat Mass Transf 2019;137:990–1000.
[68] Guo H, Li Y, Wang B, Zhang H, Xu H. Numerical investigation on flashing jet behaviors of single-hole GDI injector. Int J Heat Mass Transf 2019;130:50–9.
[69] Rachakonda SK, Paydarfar A, Schmidt DP. Prediction of spray collapse in multi-hole gasoline direct-injection fuel injectors. Int J Engine Res 2018;20:18–33.
[70] Price C, Hamzehloo A, Aleiferis P, Richardson D. Aspects of numerical modelling of flash-boiling fuel sprays. SAE International; 2015.
[71] Price C, Hamzehloo A, Aleiferis P, Richardson D. An approach to modeling flash-boiling fuel sprays for direct-injection spark-ignition engines. Atomiz Sprays 2016;26:1197–239.
[72] Huang Y, Hong G, Zhou J. Numerical modelling of ethanol direct injection (EDI) sprays of a multi-hole injector under non-evaporating, transition and flash-boiling conditions. SAE International; 2017.
[73] Senda J, Hojyo Y, Fujimoto H. Modelling of atomization process in flash boiling spray. SAE Trans 1994;103:1026–40.
[74] Adachi M, McDonell VG, Tanaka D, Senda J, Fujimoto H. Characterization of fuel vapor concentration inside a flash boiling spray. SAE technical paper. 1997.
[75] Kawano D, Goto Y, Odaka M, Senda J. Modeling atomization and vaporization processes of flash-boiling spray. SAE technical paper. 2004.
[76] Zeng Y, Lee C-FF. An atomization model for flash boiling sprays. Combust Sci Technol 2001;169:45–67.
[77] Kim T, Park S. Modeling flash boiling breakup phenomena of fuel spray from multi-hole type direct-injection spark-ignition injector for various fuel components. Energy Convers Manage 2018;160:165–75.
[78] Ra Y, Reitz RD. A vaporization model for discrete multi-component fuel sprays. Int J Multiphase Flow 2009;35:101–17.
[79] Montanaro A, Allocca L, Lazzaro M. Iso-octane spray from a GDI multi-hole injector under non- and flash boiling conditions. SAE International; 2017.
[80] Zhang M, Xu M, Zhang Y, Zhang G, Cleary DJ. Flow-field investigation of multi-hole superheated sprays using high-speed PIV. Part I. Cross-sectional direction. Atomiz Sprays 2012;22:983–95.

[81] Zhang M, Xu M, Zhang Y, Zhang G, Cleary DJ. Flow-field investigation of multihole superheated sprays using high-speed PIV. Part II. axial direction. Atomiz Sprays 2013;23:119–40.
[82] Wei H, Gao D, Zhou L, Feng D, Chen C, Pei Z. Experimental analysis on spray development of 2-methylfuran–gasoline blends using multi-hole DI injector. Fuel 2016;164:245–53.
[83] Huang Y, Huang S, Huang R, Hong G. Spray and evaporation characteristics of ethanol and gasoline direct injection in non-evaporating, transition and flash-boiling conditions. Energy Convers Manage 2016;108:68–77.
[84] Wu S, Xu M, Hung DLS, Pan H. In-nozzle flow investigation of flash boiling fuel sprays. Appl Therm Eng 2017;117:644–51.
[85] Wu S, Xu M, Yang S, Yin P. Contrary effects of nozzle length on spray primary breakup under subcooled and superheated conditions. SAE International; 2018.
[86] Zhang X, He Z, Wang Q, Tao X, Zhou Z, Xia X, et al. Effect of fuel temperature on cavitation flow inside vertical multi-hole nozzles and spray characteristics with different nozzle geometries. Exp Therm Fluid Sci 2018;91:374–87.
[87] Serras-Pereira J, van Romunde Z, Aleiferis PG, Richardson D, Wallace S, Cracknell RF. Cavitation, primary break-up and flash boiling of gasoline, iso-octane and n-pentane with a real-size optical direct-injection nozzle. Fuel 2010;89:2592–607.